an intracellular NH_2-terminus, two repeats of six transmembrane domains (M1 and M2) and two cytoplasmic catalytic domains of ~40 kDa each (C1 and C2). Crystal structure-coupled with biochemical data indicate that two cytosolic domains form the catalytic core pocket, and ATP binds at one of two pseudosymmetric binding sites at the C1-C2 interface (10, 75). Forskolin binds in two almost equivalent pockets at either end of C1 and C2 domains (87). For the isoforms of AC1, AC2, and AC5, expression of either the α-half (M1/C1) or the β-half (M2/C2) of the molecule alone is insufficient to generate enzymatic activity. The specificity of AC response likely depends on the creation of intracellular microdomains containing signaling molecules. In the submicromolar range of Ca^{2+}, the sensitivity of ACs for Ca^{2+} is coupled with distinct subcellular localization of Ca^{2+}-sensitive AC isoforms (82, 83), suggesting a temporally and spatially distinct pattern of cAMP signaling, depending on the localization of ACs in Ca^{2+} microdomains within the plasma membrane or cytoplasm. For instance, studies in overexpression models suggested that AC8 may augment cardiac contractility by preferentially activating Ca^{2+} loading of sarcoplasmic reticulum through cAMP compartmentation, rather than enhancing Ca^{2+} influx via L-type Ca^{2+} channels (21). Dyachok et al. (12) suggested that oscillations of cAMP lead to selective target activation by restricting the spatial redistribution of PKA (12). β-Adrenergic receptors (β-AR) are selectively located in plasma membrane lipid raft microdomains, resulting in more efficient coupling to AC compared with nonlipid raft microdomain receptors, such as the E-prostanoid-2 receptor. Signaling modules that include AC isoforms also contain A kinase anchoring proteins (AKAPs), PKA, and anchored phosphodiesterases to provide microdomains of cAMP production and signaling (2, 34, 82, 86).

Since AC signaling in general and AC5 signaling in particular have been extensively reviewed (31, 56, 67), this review will focus on AC5 and its regulation of responses to chronic stress and disease. We will also provide a brief overview of the potential translational direction of this work, discussing some of our recent findings with a pharmacological AC5 inhibitor.

β-AR-G Protein-AC-cAMP Signaling Pathway

The β-AR-G protein-AC-cAMP signaling pathway is one of the major pathophysiological mechanisms for regulation of cardiac function (31, 45, 47, 78). By targeting Ca^{2+} handling proteins, it provides strong inotropic and chronotropic response in times of need, such as in fight or flight (22, 48, 70, 72). Throughout much of the 20th century, it was believed that stimulation of this pathway could provide inotropic support and should be used in heart failure therapy. It was shown that transgenic (Tg) mice with up to 60-fold overexpression of β_2-AR had enhanced cardiac function without signs of cardiac pathology (46, 51). Furthermore, β_2-AR transgene experiments showed improvement in function in failing rabbit hearts (76). More recent work with adenoviral-mediated β_2-AR transgene overexpression demonstrated enhanced cardiac function in a rat model of heart failure (65). However, the concept of treating heart failure with chronically enhanced β-AR stimulation became controversial when patients responded positively to acute β-AR inotropic therapy, particularly with dopamine and dobutamine, but had poor outcomes when on prolonged inotropic therapy (14, 44, 55). An experimental study that first highlighted the adverse effects of chronic β-AR signaling was shown in $G_{s\alpha}$ Tg mice (36). Although these animals had higher responsiveness to isoproterenol (Iso) when young, a picture of cardiomyopathy developed as they aged, including myocardial hypertrophy, fibrosis and necrosis, and depression of cardiac function (1, 36, 37). Later studies using β_1-AR (15, 16, 63)- and β_2-AR (11, 63)-overexpressed models confirmed these findings, i.e., hyperfunction at young age and deterioration of function with aging. These studies (1, 11, 15, 16, 36, 37, 63) in combination with clinical studies showing poor outcomes in patients on β-AR agonists (14, 44, 55) and Bristow's classical study in *The New England Journal of Medicine* demonstrating desensitization of the β-AR in patients with heart failure (4) changed the paradigm from treating patients with heart failure with β-AR agonists to antagonists (7, 8, 30, 60, 68). Heart failure still remains as the leading cause of mortality and morbidity in the United States. For this reason, targeting components distal to the β-AR signaling, such as ACs, will be important for the development of future treatment of heart failure.

AC in the Heart

Whereas AC2, -3, -4, -5/6, and -7 are detected in rat cardiac fibroblasts (59), AC5 and AC6 are the two major isoforms expressed in the adult mammalian heart (23, 35). Both AC5 and AC6 regulate heart rate and contractility, but AC6 plays a more significant role at baseline in view of the relatively minor reduction in AC content and corresponding reductions in cardiac contractility observed in AC5 knockout (AC5-KO) hearts (58). However, the role of these two major isoforms in the heart in mediating the response to cardiac stress is controversial. In this article, we first review the studies demonstrating an adverse effect of overexpression of AC5 and beneficial effects of disrupting AC5 on cardiomyopathies induced by chronic Iso stimulation, aging, and pressure overload in either AC5-Tg or AC5-KO mice. This leads to a discussion of other factors involved in AC5 protection against aging, e.g., metabolism and diabetes. Since not all studies are in agreement, we then discuss those with an opposite point of view and reconcile the differences. The controversial studies on AC6 overexpression and disruption are beyond the scope of this review, which focuses on AC5.

Regulation of Cardiomyopathy by AC5

Chronic catecholamine cardiomyopathy. Chronic Iso increased oxidative stress and induced a more severe cardiomyopathy in AC5-Tg compared with wild-type (WT) mice, as reflected by a greater impairment of left ventricular (LV) ejection fraction (EF) along with greater LV dilation and increased fibrosis, apoptosis, and hypertrophy (41) (Fig. 1, *A* and *B*). LV EF fell more ($P < 0.05$) in AC5-Tg than WT mice (-35 ± 2 vs. $-18 \pm 1\%$). Oxidative stress induced by chronic Iso was greater in AC5-Tg hearts, whereas protein expression of manganese superoxide dismutase (MnSOD), which protects against oxidative stress, was reduced by 36%, suggesting that the increased severity of the cardiomyopathy in AC5-Tg may have resulted as a consequence of decreased MnSOD expression. This was confirmed by mating AC5-Tg with MnSOD-Tg mice. These bigenic mice no longer responded to chronic Iso with more severe cardiomyopathy than WT mice. In fact, LV EF fell less in AC5-Tg × MnSOD-Tg ($-13 \pm 1\%$) versus either AC5-Tg or WT mice. LV EF fell similarly in

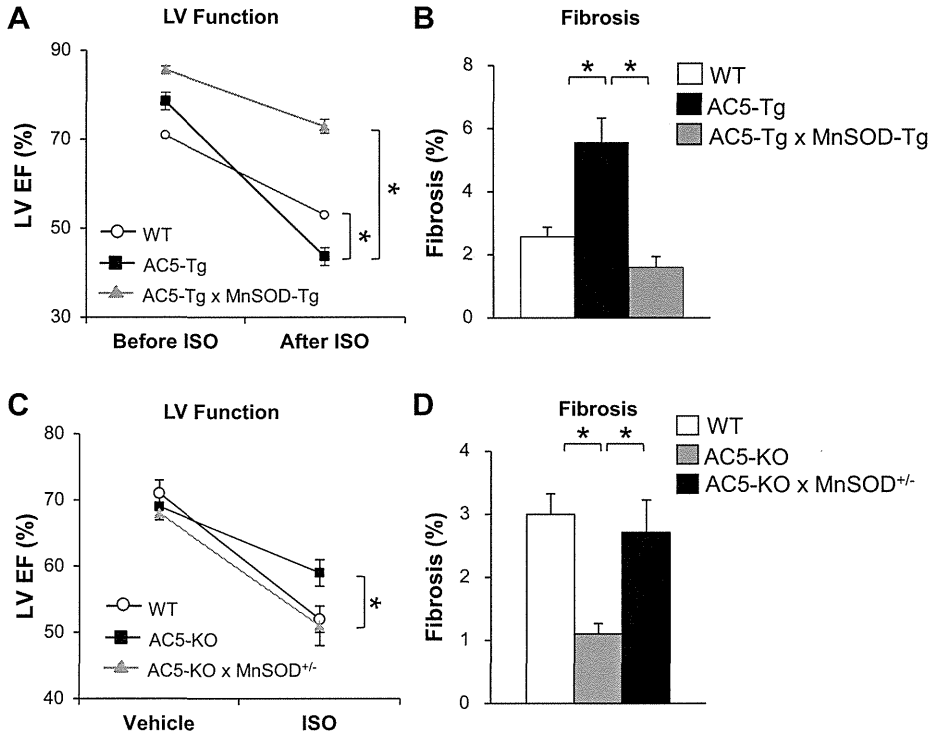

Fig. 1. *A* and *B*: chronic isoproterenol (Iso) exacerbated cardiomyopathy in transgenic overexpression of adenylyl cyclase 5 in cardiomyocytes of the heart (AC5-Tg) compared with wild-type (WT), and the cardiomyopathy was rescued by mating the AC5-Tg mice with MnSOD-Tg (AC5-Tg × MnSOD-Tg) mice (41). *C* and *D*: downregulation of MnSOD eliminated the protective effects of AC5-knockout (KO) with chronic Iso. LV, left ventricular; EF, ejection fraction. $^*P < 0.05$ (41). Figures used are modified with permission from Lai et al. (41).

MnSOD-Tg alone (−13 ± 2%). Conversely, AC5-KO mice are protected from the cardiomyopathy induced by chronic Iso treatment (58), as reflected by less of a reduction with chronic Iso ($P < 0.05$) in AC5-KO than WT (−10 ± 2 vs. −19 ± 2%) mice, and this protection was lost in bigenic AC5-KO mice mated with MnSOD heterozygous KO mice, where LV EF fell by −18 ± 3% (Fig. 1, *C* and *D*). The decrease in LV EF with chronic Iso in the bigenic AC5-KO × MnSOD heterozygous mouse was similar to that in the MnSOD heterozygous alone (−18 ± 3 vs. −18 ± 4%). The decreases in LV EF must be interpreted with the histological changes in the heart consistent with chronic cardiomyopathy, e.g., fibrosis and apoptosis. When the data are all taken together, the picture of intensification of cardiomyopathy with AC5-Tg and protection with MnSOD-Tg or AC5-KO becomes even more apparent. We also demonstrated that AC5, but not AC6, regulates MnSOD at the transcriptional level via the sirtuin 1/forkhead box O3a pathway (Fig. 2). Thus the cardiomyopathy induced by chronic catecholamine stress is intensified in AC5-Tg by inhibiting sirtuin 1/forkhead box O3a, which downregulates MnSOD transcription, resulting in oxidative stress intolerance (41).

Chronic pressure-overload cardiomyopathy. Cardiac hypertrophy in response to pressure overload is a double- edged sword; on the one-hand it compensates for the pressure overload, whereas on the other hand LV hypertrophy impairs LV function (26, 40), eventually leading to heart failure. AC5-KO mice tolerated chronic pressure overload better than WT, with improved LV function, less fibrosis, and apoptosis in the heart (57).

We previously showed that AC5 and AC6 have opposite protein expression levels in response to pressure overload LV hypertrophy, e.g., an upregulation of AC5 and a downregulation of AC6 (33), suggesting unique regulatory pathways for AC5 in response to chronic pressure overload cardiomyopathy. In addition, it was reported that myocardial AC5 mRNA expression was increased from 5–12 wk in spontaneously hypertensive rats, which was accompanied by development of LV hypertrophy and hypertension (20). Recently, from mi-

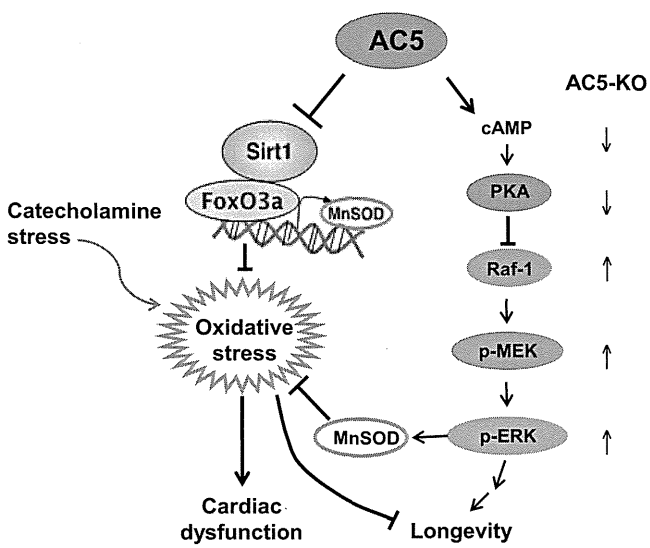

Fig. 2. Signaling diagram for AC5 mediating cardiac stress and longevity. *Left*: cardiac dysfunction: signaling diagram for AC5 regulation of MnSOD transcriptionally through the sirtuin 1/forkhead box O3a (SIRT1/FoxO3a) pathway is shown. Imbalance between reactive oxygen species production and the intracellular antioxidant system results in the intolerance of AC5-Tg to stress (41). *Right*: longevity: disruption of AC5 activates the Raf/MEK/ERK signaling pathway. The activation of ERK activates antioxidative stress and cell survival mechanism, which leads to longevity in AC5-KO mice (85). Arrows indicate the direction of signaling. Figures used are modified with permission from Lai et al. (41) and Yan et al. (85).

croarray analysis we found several genes in AC5-Tg hearts related to LV hypertrophy, which was similar to those in a public data set for pressure overload LV hypertrophy and that the transcription factor binding site of nuclear factor of activated t-cells (NFAT), a key prohypertrophic pathway (3, 81), is enriched in AC5-Tg hearts even at baseline, suggesting that cardiac overexpression of AC5 predisposes the heart to LV hypertrophy (61), which is not observed in AC6-Tg hearts (27). Another mechanism mediating the role of AC5 and hypertrophy is the muscle protein AKAP (mAKAPβ), which is required for the cAMP second messenger controlling cardiac myocyte hypertrophy. AC5 binds selectively and directly to a unique NH_2-terminal site on mAKAPβ, but not AC6 (39).

Aging cardiomyopathy. The genetically engineered mouse model in which type 5 AC was knocked out, i.e., AC5-KO mice, have increased median life span of ~30% (Fig. 3*A*) and are protected from aging-induced cardiomyopathy (85), including decreased LV hypertrophy, decreased fibrosis, and decreased apoptosis compared with WT as they age (Fig. 3*B*). Using a proteomic-based approach, we demonstrated a significant activation of the Raf/MEK/ERK signaling pathway, which results in protection from oxidative stress, leading to longevity in AC5-KO mice (Fig. 2). In addition to the prolonged life and protection against aging cardiomyopathy in AC5-KO mice, this model also exhibits protection against the osteoporosis of aging (85). Furthermore, both young and old AC5-KO mice had better exercise endurance than WT mice of the corresponding age. These beneficial effects of AC5 disruption on aging are synergistic in clinical relevance of AC5 inhibition, since elderly patients have an increased prevalence of heart failure (42, 43).

AC5-KO model vs. calorie restriction models of longevity. Calorie restriction (CR) is the most widely studied model of longevity (5, 50, 71). Our hypothesis was that superimposing CR on the AC5-KO would combine their potentially different mechanisms mediating longevity resulting in a superlongevity model. This hypothesis was not correct, and superimposing CR on the AC5-KO was uniformly lethal within a month (79, 84). AC5-KO mice on CR developed a syndrome similar to starvation, as evidenced by greater decrease in body weight, blood glucose, fat and glycogen storage, and greater increase in ketone bodies than either AC5-KO or CR alone. Accordingly, we adopted the converse hypothesis that the longevity mechanisms were similar in the two models. To test this, we recently compared AC5-KO model with CR in terms of physical phenotype as well as metabolic and gene expression profiles (84). Similar to the mice on CR, AC5-KO mice exhibit a lower body weight, reduced fat accumulation (Fig. 4*B*) and glycogen stores, and lower fasting blood glucose levels. However, in contrast to CR with restricted food intake, AC5-KO mice eat more compared with their WT littermates. Microarray analysis revealed a remarkable similarity of gene profiles between AC5-KO and CR mice in the heart, skeletal muscle, and brain (Fig. 4*A*). Many tissue-specific pathways in the regulation of metabolism, longevity, and stress resistance overlap in the AC5-KO and CR mouse models, including sensory perception in heart and brain, muscle function in skeletal muscle, and lipid metabolism in liver (Fig. 4*C*). Importantly, the similarly regulated genes and pathways for AC5-KO and CR will begin to establish a unified theory for longevity, stress resistance, and potentially for diabetes and obesity.

Diabetic cardiomyopathy. A key extrapolation from the above study comparing AC5-KO and CR is that both models of longevity protect against glucose intolerance and insulin resistance (24, 32, 80, 84) and, taken together with AC5-KO's ability to protect against pressure overload and catecholamine cardiomyopathy, raises the likely probability that AC5-KO also might protect against diabetic cardiomyopathy. Even at

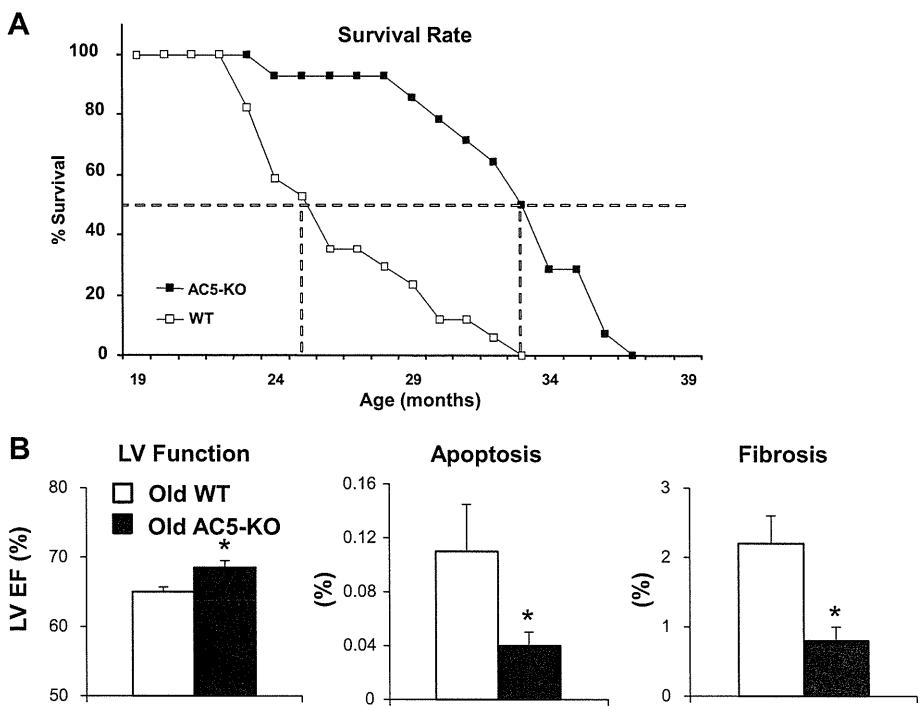

Fig. 3. Disruption of AC5 protects against cardiac stress. *A*: effects of AC5-KO on longevity (85). *B*: effects of AC5-KO on aging cardiomyopathy. LV EF, apoptosis, and fibrosis were significantly different in old AC5-KO vs. old WT. $*P < 0.05$. Figures used are modified with permission from Yan et al. (85).

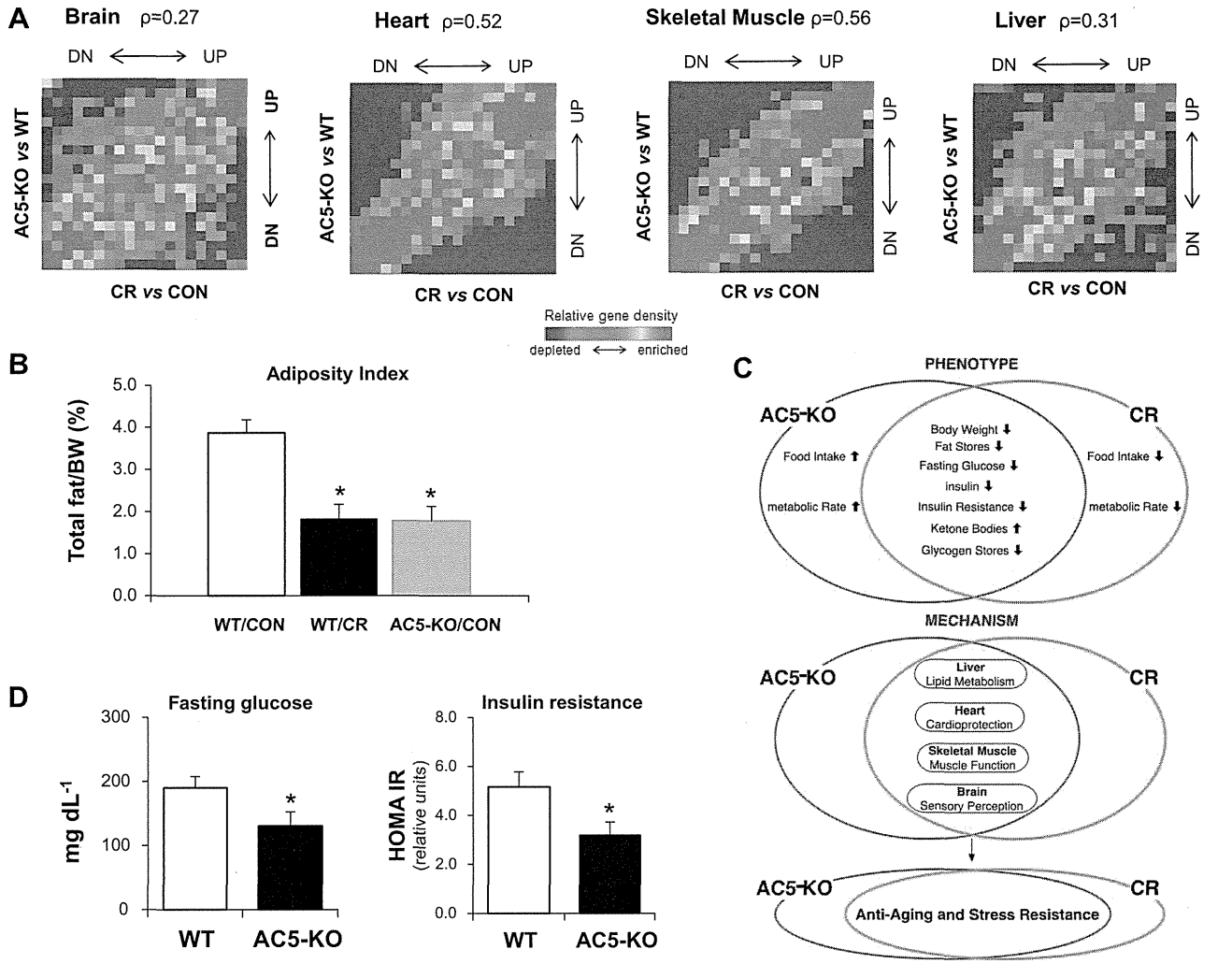

Fig. 4. Common mechanisms for calorie restriction (CR) and AC5-KO models. *A*: microarray analysis revealed a similarity between the changes in gene expression between AC5-KO and CR mice. Con, control diet; DN, down; UP, up (84). *B*: adiposity index showed that AC5-KO mice have less fat accumulation. WT/Con, WT on control diet; WT/CR, WT on calorie restriction; AC5-KO/CON, AC5-KO on control diet. *$P < 0.05$ (84). BW, body weight. *C*: differences and similarities between AC5-KO and CR mice are shown in the metabolic phenotypes and the common mechanisms regarding resistance to aging and stress (84). *D*: fasting glucose level and insulin resistance of AC5-KO and WT following 6 h fasting. ; BW, body weight; HOMA IR, homeostasis model of assessment-insulin resistance. *$P < 0.05$ (84). Figure used is modified with permission from Yan et al. (84).

baseline, in the absence of a high-fat diet, levels of fasting glucose and insulin resistance were lower in AC5-KO (Fig. 4*D*). Our preliminary results suggest that AC5-KO protects against diabetic cardiomyopathy (32). When the AC5-KO and their WT were placed on a high-fat diet, the WT rapidly developed a reduction in cardiac function with histopathological evidence of cardiomyopathy, as typically reported in the literature (6, 18, 62). However, the AC5-KO was protected against high-fat diet-induced cardiomyopathy (32). These observations underlie several important and clinical relevant questions. For example, is the protection of the cardiomyopathy due to an action of AC5-KO on the heart, i.e., the target organ of the cardiomyopathy, or is it indirectly due to an action on metabolism, i.e., the initiating cause of the cardiomyopathy? These and other related investigations are currently underway.

Controversy in role of AC5 in the heart. Not all studies have found that overexpression of AC5 is deleterious or that its disruption is salutary. For example, when AC5 is overexpressed in the heart, LV function is improved as well as the response to exercise (17). This is not particularly surprising since increasing any component of the β-AR signaling pathway, even at the level of the β-receptor, improves cardiac performance at baseline and in the response to exercise, as we have also observed in our AC5-Tg models. The adverse effects appear much later with chronically enhanced β-AR signaling. The bottom line is that patients with heart failure respond favorably to β-AR blockade over the long haul but have increased mortality with chronically enhanced β-AR stimulation. A more controversial finding is that AC5-Tg was able to rescue $G_{\alpha q}$ overexpression-induced cardiomyopathy (74) but not cardiomyopathy induced by cardiac overexpression of β-AR (64). Conversely, AC5-KO mice were not able to rescue $G_{\alpha q}$ overexpression-induced cardiomyopathy (77). These seemingly different results from rescue of cardiomyopathy (57,

58, 77) are not likely due to different backgrounds in the KO mice, but rather reconciliation of the differences in these studies is more apparent when understanding the signaling pathways. For example, Tg mice with cardiac-specific overexpression of $G_{\alpha q}$ showed that the cardiomyopathy was mediated by PKC with a significant reduction in AC5. Therefore, it is logical that replacing AC5 in this situation would be beneficial and that reducing it further, as with the AC5-KO, would not be beneficial. However, β_1-AR or chronic Iso-stimulated cardiomyopathy is mediated by PKA with increased levels of AC5 (58). These results, taken together, support our hypothesis that chronically elevated levels of AC activation, like β-AR (11, 16, 63) or $G_{s\alpha}$ (1, 36, 37), are deleterious and facilitate development of cardiomyopathy. In contrast, when a cardiomyopathy develops associated with reduced levels of AC5, restoration of AC5 expression may be beneficial for normal cardiac function under these conditions.

Clinical Relevance of AC5

Although hundreds, if not thousands, of novel and exciting discoveries have been made by alterations in genes in genetically engineered mice, relatively few have translated into improving clinical care. One reason for the lack of success is that it is difficult to overexpress or delete a gene in patients. Therefore, the goal becomes to have a pharmacological analog of the altered gene that can be safely delivered to patients. A current goal of our laboratory is to translate the beneficial effects of the AC5-KO model to clinical therapy. In this connection, while screening for a commercially available drug for the AC5 inhibition, adenine-9-β-D-arabinofuranoside (Ara-A; Vidarabine) showed a selective inhibition of AC5. Recent studies in our laboratory demonstrated that Ara-A selectively inhibits AC5 activity in AC5-Tg mice, but not in AC6-Tg mice. In cardiac membrane preparations with Iso stimulation, Ara-A (10 μM) reduced cAMP production much more in AC5-Tg (49%) than in WT and not at all in AC5-KO (38). Ara-A was originally developed as an antiviral drug, which was approved by the United States Food and Drug Administration. It has been clinically used for treatment of herpes virus infection, but it was found to be less efficient for viral therapy than the newer drug, acyclovir. We also found that this pharmacological AC5 inhibitor recapitulates the favorable effects of AC5 disruption and ameliorated the development of cardiomyopathy and heart failure induced by either permanent coronary artery occlusion or chronic catecholamine infusion (38). Ara-A significantly improved the survival rate and LV function compared with vehicle after 3 wk of coronary artery occlusion, and these beneficial effects of Ara-A were abolished by U0126, a MEK inhibitor, suggesting the involvement of the downstream MEK-ERK pathway of AC5 (38). This is significant since the same signaling pathway was found mediating the longevity in AC5-KO (85). In heart failure, Ara-A has also been shown to reduce autophagy by inhibition of AMPK (49). Since toxicology for the drug has found little to be contraindicated in heart failure and since adverse effects were only manifest with very high chronic doses, low dose Ara-A is a strong candidate for a clinical trial for heart failure since it selectively inhibits AC5, has been shown to protect against heart failure without adverse effects, and has been already approved by the United States Food and Drug Administration. One potential limitation to this drug is that only an intravenous formulation is currently available. Accordingly, drug discovery studies will have to be pursued for oral delivery and optimizing the compound for heart failure applications.

Conclusions

There are several take-home messages. First, although AC5 and AC6 are the two major isoforms in the heart, they mediate dramatically different functions, particularly in response to stress. Second, although AC5 is one of the major cardiac isoforms of AC, potentially its most important role will be in mediating diabetes, obesity, and longevity, even more so than in cardiac protection. Finally, it may be possible to translate the beneficial effects of the AC5-KO to the bedside, by using a pharmacological analog, which preferentially inhibits AC5.

GRANTS

This study was supported by National Institutes of Health Grants HL-093481, HL-106511, HL-033107, HL-095888, HL-069020, and AG-027211.

DISCLOSURES

S. F. Vatner and D. E. Vatner both work for Vasade Biosciences, which also has research interests in AC5 but has no intellectual property and did not provide support for this study. All research was funded by the NIH.

AUTHOR CONTRIBUTIONS

S.F.V. and D.E.V. conception and design of research; S.F.V., M.P., and L.Y. drafted manuscript; S.F.V., M.P., G.J.A.L., L.L., K.I., Y.I., J.E.P., and D.E.V. edited and revised manuscript; S.F.V. and D.E.V. approved final version of manuscript; M.P. prepared figures.

REFERENCES

1. **Asai K, Yang GP, Geng YJ, Takagi G, Bishop S, Ishikawa Y, Shannon RP, Wagner TE, Vatner DE, Homcy CJ, Vatner SF.** Beta-adrenergic receptor blockade arrests myocyte damage and preserves cardiac function in the transgenic G(salpha) mouse. *J Clin Invest* 104: 551–558, 1999.
2. **Bauman AL, Soughayer J, Nguyen BT, Willoughby D, Carnegie GK, Wong W, Hoshi N, Langeberg LK, Cooper DM, Dessauer CW, Scott JD.** Dynamic regulation of cAMP synthesis through anchored PKA-adenylyl cyclase V/VI complexes. *Mol Cell* 23: 925–931, 2006.
3. **Bourajjaj M, Armand AS, da Costa Martins P.A, Weijts B, van der Nagel R, Heeneman S, Wehrens XH, De Windt LJ.** NFATc2 is a necessary mediator of calcineurin-dependent cardiac hypertrophy and heart failure. *J Biol Chem* 283: 22295–22303, 2008.
4. **Bristow MR, Ginsburg R, Minobe W, Cubicciotti RS, Sageman WS, Lurie K, Billingham ME, Harrison DC, Stinson EB.** Decreased catecholamine sensitivity and beta-adrenergic-receptor density in failing human hearts. *N Engl J Med* 307: 205–211, 1982.
5. **Canto C, Auwerx J.** Caloric restriction, SIRT1 and longevity. *Trends Endocrinol Metab* 20: 325–331, 2009.
6. **Cao J, Sodhi K, Puri N, Monu SR, Rezzani R, Abraham NG.** High fat diet enhances cardiac abnormalities in SHR rats: protective role of heme oxygenase-adiponectin axis. *Diabetol Metab Syndr* 3: 37, 2011.
7. **CIBIS Investigators and Committees.** A randomized trial of beta-blockade in heart failure. The Cardiac Insufficiency Bisoprolol Study (CIBIS). *Circulation* 90: 1765–1773, 1994.
8. **CIBIS-II Investigators and Committees.** The Cardiac Insufficiency Bisoprolol Study I.I. (CIBIS-II): a randomized trial. *Lancet* 353: 9–13, 1999.
9. **Defer N, Best-Belpomme M, Hanoune J.** Tissue specificity and physiological relevance of various isoforms of adenylyl cyclase. *Am J Physiol Renal Physiol* 279: F400–F416, 2000.
10. **Dessauer CW, Gilman AG.** The catalytic mechanism of mammalian adenylyl cyclase. Equilibrium binding and kinetic analysis of P-site inhibition. *J Biol Chem* 272: 27787–27795, 1997.
11. **Du XJ, Gao XM, Wang B, Jennings GL, Woodcock EA, Dart AM.** Age-dependent cardiomyopathy and heart failure phenotype in mice over-

expressing beta(2)-adrenergic receptors in the heart. *Cardiovasc Res* 48: 448–454, 2000.

12. **Dyachok O, Isakov Y, Sagetorp J, Tengholm A.** Oscillations of cyclic AMP in hormone-stimulated insulin-secreting beta-cells. *Nature* 439: 349–352, 2006.
13. **Efendiev R, Dessauer CW.** A kinase-anchoring proteins and adenylyl cyclase in cardiovascular physiology and pathology. *J Cardiovasc Pharmacol* 58: 339–344, 2011.
14. **Elkayam U, Tasissa G, Binanay C, Stevenson LW, Gheorghiade M, Warnica JW, Young JB, Rayburn BK, Rogers JG, DeMarco T, Leier CV.** Use and impact of inotropes and vasodilator therapy in hospitalized patients with severe heart failure. *Am Heart J* 153: 98–104, 2007.
15. **Engelhardt S, Hein L, Dyachenkow V, Kranias EG, Isenberg G, Lohse MJ.** Altered calcium handling is critically involved in the cardiotoxic effects of chronic beta-adrenergic stimulation. *Circulation* 109: 1154–1160, 2004.
16. **Engelhardt S, Hein L, Wiesmann F, Lohse MJ.** Progressive hypertrophy and heart failure in beta1-adrenergic receptor transgenic mice. *Proc Natl Acad Sci USA* 96: 7059–7064, 1999.
17. **Esposito G, Perrino C, Ozaki T, Takaoka H, Defer N, Petretta MP, De Angelis MC, Mao L, Hanoune J, Rockman HA, Chiariello M.** Increased myocardial contractility and enhanced exercise function in transgenic mice overexpressing either adenylyl cyclase 5 or 8. *Basic Res Cardiol* 103: 22–30, 2008.
18. **Fang CX, Dong F, Thomas DP, Ma H, He L, Ren J.** Hypertrophic cardiomyopathy in high-fat diet-induced obesity: role of suppression of forkhead transcription factor and atrophy gene transcription. *Am J Physiol Heart Circ Physiol* 295: H1206–H1215, 2008.
19. **Feldman AM.** Adenylyl cyclase: a new target for heart failure therapeutics. *Circulation* 105: 1876–1878, 2002.
20. **Fujino T, Hasebe N, Kawabe J, Fujita M, Fukuzawa J, Tobise K, Kikuchi K.** Effect of beta-adrenoceptor antagonist and angiotensin-converting enzyme inhibitor on hypertension-associated changes in adenylyl cyclase type V messenger RNA expression in spontaneously hypertensive rats. *J Cardiovasc Pharmacol* 41: 720–725, 2003.
21. **Georget M, Mateo P, Vandecasteele G, Jurevicius J, Lipskaia L, Defer N, Hanoune J, Hoerter J, Fischmeister R.** Augmentation of cardiac contractility with no change in L-type Ca^{2+} current in transgenic mice with a cardiac-directed expression of the human adenylyl cyclase type 8 (AC8). *FASEB J* 16: 1636–1638, 2002.
22. **Gerhardstein BL, Puri TS, Chien AJ, Hosey MM.** Identification of the sites phosphorylated by cyclic AMP-dependent protein kinase on the beta 2 subunit of L-type voltage-dependent calcium channels. *Biochemistry* 38: 10361–10370, 1999.
23. **Gottle M, Geduhn J, Konig B, Gille A, Hocherl K, Seifert R.** Characterization of mouse heart adenylyl cyclase. *J Pharmacol Exp Ther* 329: 1156–1165, 2009.
24. **Gresl TA, Colman RJ, Roecker EB, Havighurst TC, Huang Z, Allison DB, Bergman RN, Kemnitz JW.** Dietary restriction and glucose regulation in aging rhesus monkeys: a follow-up report at 8.5 yr. *Am J Physiol Endocrinol Metab* 281: E757–E765, 2001.
25. **Gros R, Ding Q, Chorazyczewski J, Pickering JG, Limbird LE, Feldman RD.** Adenylyl cyclase isoform-selective regulation of vascular smooth muscle proliferation and cytoskeletal reorganization. *Circ Res* 99: 845–852, 2006.
26. **Grossman W, Jones D, McLaurin LP.** Wall stress and patterns of hypertrophy in the human left ventricle. *J Clin Invest* 56: 56–64, 1975.
27. **Guellich A, Gao S, Hong C, Yan L, Wagner TE, Dhar SK, Ghaleb B, Hittinger L, Iwatsubo K, Ishikawa Y, Vatner SF, Vatner DE.** Effects of cardiac overexpression of type 6 adenylyl cyclase affects on the response to chronic pressure overload. *Am J Physiol Heart Circ Physiol* 299: H707–H712, 2010.
28. **Haber N, Stengel D, Defer N, Roeckel N, Mattei MG, Hanoune J.** Chromosomal mapping of human adenylyl cyclase genes type III, type V and type VI. *Hum Genet* 94: 69–73, 1994.
29. **Hakonarson H, Grunstein MM.** Regulation of second messengers associated with airway smooth muscle contraction and relaxation. *Am J Respir Crit Care Med* 158: S115–S122, 1998.
30. **Hjalmarson A, Goldstein S, Fagerberg B, Wedel H, Waagstein F, Kjekshus J, Wikstrand J, El Allaf D, Vitovec J, Aldershvile J, Halinen M, Dietz R, Neuhaus KL, Janosi A, Thorgeirsson G, Dunselman PH, Gullestad L, Kuch J, Herlitz J, Rickenbacher P, Ball S, Gottlieb S, Deedwania P.** Effects of controlled-release metoprolol on total mortality, hospitalizations, and well-being in patients with heart failure: the Metoprolol CR/XL Randomized Intervention Trial in congestive heart failure (MERIT-HF). MERIT-HF Study Group. *JAMA* 283: 1295–1302, 2000.
31. **Ho D, Yan L, Iwatsubo K, Vatner DE, Vatner SF.** Modulation of beta-adrenergic receptor signaling in heart failure and longevity: targeting adenylyl cyclase type 5. *Heart Fail Rev* 15: 495–512, 2010.
32. **Ho D, Yan L, Zhao X, Bravo C, Stanley W, Vatner DE, Pessin J, Vatner SF.** Disruption of adenylyl cyclase type 5, a novel target for obesity, diabetes and diabetic cardiomyopathy (Abstract). *Circulation* 126: A19323 2012.
33. **Hu CL, Chandra R, Ge H, Pain J, Yan L, Babu G, Depre C, Iwatsubo K, Ishikawa Y, Sadoshima J, Vatner SF, Vatner DE.** Adenylyl cyclase type 5 protein expression during cardiac development and stress. *Am J Physiol Heart Circ Physiol* 297: H1776–H1782, 2009.
34. **Iancu RV, Jones SW, Harvey RD.** Compartmentation of cAMP signaling in cardiac myocytes: a computational study. *Biophys J* 92: 3317–3331, 2007.
35. **Ishikawa Y, Katsushika S, Chen L, Halnon NJ, Kawabe J, Homcy CJ.** Isolation and characterization of a novel cardiac adenylylcyclase cDNA. *J Biol Chem* 267: 13553–13557, 1992.
36. **Iwase M, Bishop SP, Uechi M, Vatner DE, Shannon RP, Kudej RK, Wight DC, Wagner TE, Ishikawa Y, Homcy CJ, Vatner SF.** Adverse effects of chronic endogenous sympathetic drive induced by cardiac GS alpha overexpression. *Circ Res* 78: 517–524, 1996.
37. **Iwase M, Uechi M, Vatner DE, Asai K, Shannon RP, Kudej RK, Wagner TE, Wight DC, Patrick TA, Ishikawa Y, Homcy CJ, Vatner SF.** Cardiomyopathy induced by cardiac Gsα overexpression. *Am J Physiol Heart Circ Physiol* 272: H585–H589, 1997.
38. **Iwatsubo K, Bravo C, Uechi M, Baljinnyam E, Nakamura T, Umemura M, Lai L, Gao S, Yan L, Zhao X, Park M, Qiu H, Okumura S, Iwatsubo M, Vatner DE, Vatner SF, Ishikawa Y.** Prevention of heart failure in mice by an antiviral agent that inhibits type 5 cardiac adenylyl cyclase. *Am J Physiol Heart Circ Physiol* 302: H2622–H2628, 2012.
39. **Kapiloff MS, Piggott LA, Sadana R, Li J, Heredia LA, Henson E, Efendiev R, Dessauer CW.** An adenylyl cyclase-mAKAPbeta signaling complex regulates cAMP levels in cardiac myocytes. *J Biol Chem* 284: 23540–23546, 2009.
40. **Koren MJ, Devereux RB, Casale PN, Savage DD, Laragh JH.** Relation of left ventricular mass and geometry to morbidity and mortality in uncomplicated essential hypertension. *Ann Intern Med* 114: 345–352, 1991.
41. **Lai L, Yan L, Gao S, Hu CL, Ge H, Davidow A, Park M, Bravo C, Iwatsubo K, Ishikawa Y, Auwerx J, Sinclair DA, Vatner SF, Vatner DE.** Type 5 adenylyl cyclases increases oxidative stress by transcriptional regulation of MnSOD via the SIRT1/FoxO3a pathway. *Circulation* 127: 1692–1701, 2013.
42. **Lakatta EG.** Age-associated cardiovascular changes in health: impact on cardiovascular disease in older persons. *Heart Fail Rev* 7: 29–49, 2002.
43. **Lakatta EG.** Arterial and cardiac aging: major shareholders in cardiovascular disease enterprises: Part III: cellular and molecular clues to heart and arterial aging. *Circulation* 107: 490–497, 2003.
44. **Lambertz H, Meyer J, Erbel R.** Long-term hemodynamic effects of prenalterol in patients with severe congestive heart failure. *Circulation* 69: 298–305, 1984.
45. **Lee GJ, Yan L, Vater DE, Vatner SF.** β-Adrenergic receptor signaling in heart failure. In: *Cardiac Remodeling: Molecular Mechanisms,* edited by Jugdutt BI and Dhalla NS. New York: Springer, 2013.
46. **Liggett SB, Tepe NM, Lorenz JN, Canning AM, Jantz TD, Mitarai S, Yatani A, Dorn GW, 2nd.** Early and delayed consequences of beta(2)-adrenergic receptor overexpression in mouse hearts: critical role for expression level. *Circulation* 101: 1707–1714, 2000.
47. **Lohse MJ, Engelhardt S, Eschenhagen T.** What is the role of beta-adrenergic signaling in heart failure? *Circ Res* 93: 896–906, 2003.
48. **Marx SO, Reiken S, Hisamatsu Y, Jayaraman T, Burkhoff D, Rosemblit N, Marks AR.** PKA phosphorylation dissociates FKBP12.6 from the calcium release channel (ryanodine receptor): defective regulation in failing hearts. *Cell* 101: 365–376, 2000.
49. **Matsui Y, Takagi H, Qu X, Abdellatif M, Sakoda H, Asano T, Levine B, Sadoshima J.** Distinct roles of autophagy in the heart during ischemia and reperfusion: roles of AMP-activated protein kinase and Beclin 1 in mediating autophagy. *Circ Res* 100: 914–922, 2007.
50. **Mattison JA, Roth GS, Beasley TM, Tilmont EM, Handy AM, Herbert RL, Longo DL, Allison DB, Young JE, Bryant M, Barnard D, Ward WF, Qi W, Ingram DK, de Cabo R.** Impact of caloric restriction

on health and survival in rhesus monkeys from the NIA study. *Nature* 489: 318–321, 2012.

51. **Milano CA, Allen LF, Rockman HA, Dolber PC, McMinn TR, Chien KR, Johnson TD, Bond RA, Lefkowitz RJ.** Enhanced myocardial function in transgenic mice overexpressing the beta 2-adrenergic receptor. *Science* 264: 582–586, 1994.
52. **Mons N, Guillou JL, Jaffard R.** The role of Ca^{2+}/calmodulin-stimulable adenylyl cyclases as molecular coincidence detectors in memory formation. *Cell Mol Life Sci* 55: 525–533, 1999.
53. **Muller G, Wied S, Over S, Frick W.** Inhibition of lipolysis by palmitate, H_2O_2 and the sulfonylurea drug, glimepiride, in rat adipocytes depends on cAMP degradation by lipid droplets. *Biochemistry* 47: 1259–1273, 2008.
54. **Neves MJ, Terenzi HF.** In vivo control of gluconeogenesis in wild-type Neurospora crassa and in the adenylate cyclase-deficient cr-1 (crisp) mutant. *J Bacteriol* 171: 1767–1771, 1989.
55. **O'Connor CM, Gattis WA, Uretsky BF, Adams KF Jr, McNulty SE, Grossman SH, McKenna WJ, Zannad F, Swedberg K, Gheorghiade M, Califf RM.** Continuous intravenous dobutamine is associated with an increased risk of death in patients with advanced heart failure: insights from the Flolan International Randomized Survival Trial (FIRST). *Am Heart J* 138: 78–86, 1999.
56. **Okumura S, Suzuki S, Ishikawa Y.** New aspects for the treatment of cardiac diseases based on the diversity of functional controls on cardiac muscles: effects of targeted disruption of the type 5 adenylyl cyclase gene. *J Pharm Sci* 109: 354–359, 2009.
57. **Okumura S, Takagi G, Kawabe J, Yang G, Lee MC, Hong C, Liu J, Vatner DE, Sadoshima J, Vatner SF, Ishikawa Y.** Disruption of type 5 adenylyl cyclase gene preserves cardiac function against pressure overload. *Proc Natl Acad Sci USA* 100: 9986–9990, 2003.
58. **Okumura S, Vatner DE, Kurotani R, Bai Y, Gao S, Yuan Z, Iwatsubo K, Ulucan C, Kawabe J, Ghosh K, Vatner SF, Ishikawa Y.** Disruption of type 5 adenylyl cyclase enhances desensitization of cyclic adenosine monophosphate signal and increases Akt signal with chronic catecholamine stress. *Circulation* 116: 1776–1783, 2007.
59. **Ostrom RS, Naugle JE, Hase M, Gregorian C, Swaney JS, Insel PA, Brunton LL, Meszaros JG.** Angiotensin II enhances adenylyl cyclase signaling via Ca^{2+}/calmodulin. Gq-Gs cross-talk regulates collagen production in cardiac fibroblasts. *J Biol Chem* 278: 24461–24468, 2003.
60. **Packer M, Bristow MR, Cohn JN, Colucci WS, Fowler MB, Gilbert EM, Shusterman NH.** The effect of carvedilol on morbidity and mortality in patients with chronic heart failure. US Carvedilol Heart Failure Study Group. *N Engl J Med* 334: 1349–1355, 1996.
61. **Park M, Park J, Lee J, Tian B, Lai L, Iwatsubo K, Ishikawa Y, Sadoshima J, Vatner DE, Vatner SF.** Cardiac overexpression of adenylyl cyclase type 5 induces left ventricular hypertrophy potentially by activating calcineurin-NFAT signaling (Abstract). *FASEB J* 365–311, 2011.
62. **Park SY, Cho YR, Kim HJ, Higashimori T, Danton C, Lee MK, Dey A, Rothermel B, Kim YB, Kalinowski A, Russell KS, Kim JK.** Unraveling the temporal pattern of diet-induced insulin resistance in individual organs and cardiac dysfunction in C57BL/6 mice. *Diabetes* 54: 3530–3540, 2005.
63. **Peter PS, Brady JE, Yan L, Chen W, Engelhardt S, Wang Y, Sadoshima J, Vatner SF, Vatner DE.** Inhibition of p38 alpha MAPK rescues cardiomyopathy induced by overexpressed beta 2-adrenergic receptor, but not beta 1-adrenergic receptor. *J Clin Invest* 117: 1335–1343, 2007.
64. **Petrashevskaya N, Gaume BR, Mihlbachler KA, Dorn GW, 2nd, Liggett SB.** Bitransgenesis with beta(2)-adrenergic receptors or adenylyl cyclase fails to improve beta(1)-adrenergic receptor cardiomyopathy. *Clin Transl Sci* 1: 221–227, 2008.
65. **Rengo G, Zincarelli C, Femminella GD, Liccardo D, Pagano G, de Lucia C, Altobelli GG, Cimini V, Ruggiero D, Perrone-Filardi P, Gao E, Ferrara N, Lymperopoulos A, Koch WJ, Leosco D.** Myocardial beta(2)-adrenoceptor gene delivery promotes coordinated cardiac adaptive remodelling and angiogenesis in heart failure. *Br J Pharmacol* 166: 2348–2361, 2012.
66. **Rosenberg D, Groussin L, Bertagna X, Bertherat. J.** cAMP pathway alterations from the cell surface to the nucleus in adrenocortical tumors. *Endocr Res* 28: 765–775, 2002.
67. **Sadana R, Dessauer CW.** Physiological roles for G protein-regulated adenylyl cyclase isoforms: insights from knockout and overexpression studies. *Neurosignals* 17: 5–22, 2009.
68. **Segev A, Mekori YA.** The Cardiac Insufficiency Bisoprolol Study II. *Lancet* 353: 1361, 1999.
69. **Shah RS, Lee HG, Xiongwei Z, Perry G, Smith MA, Castellani RJ.** Current approaches in the treatment of Alzheimer's disease. *Biomed Pharmacother* 62: 199–207, 2008.
70. **Simmerman HK, Jones LR.** Phospholamban: protein structure, mechanism of action, and role in cardiac function. *Physiol Rev* 78: 921–947, 1998.
71. **Sinclair DA.** Toward a unified theory of caloric restriction and longevity regulation. *Mech Ageing Dev* 126: 987–1002, 2005.
72. **Sulakhe PV, Vo XT.** Regulation of phospholamban and troponin-I phosphorylation in the intact rat cardiomyocytes by adrenergic and cholinergic stimuli: roles of cyclic nucleotides, calcium, protein kinases and phosphatases and depolarization. *Mol Cell Biochem* 149–150: 103–126, 1995.
73. **Sutherland EW, Rall TW.** Fractionation and characterization of a cyclic adenine ribonucleotide formed by tissue particles. *J Biol Chem* 232: 1077–1091, 1958.
74. **Tepe NM, Liggett SB.** Transgenic replacement of type V adenylyl cyclase identifies a critical mechanism of beta-adrenergic receptor dysfunction in the G alpha q overexpressing mouse. *FEBS Lett* 458: 236–240, 1999.
75. **Tesmer JJ, Sunahara RK, Gilman AG, Sprang SR.** Crystal structure of the catalytic domains of adenylyl cyclase in a complex with Gsalpha. GTPgammaS. *Science* 278: 1907–1916, 1997.
76. **Tevaearai HT, Eckhart AD, Walton GB, Keys JR, Wilson K, Koch WJ.** Myocardial gene transfer and overexpression of beta2-adrenergic receptors potentiates the functional recovery of unloaded failing hearts. *Circulation* 106: 124–129, 2002.
77. **Timofeyev V, Porter CA, Tuteja D, Qiu H, Li N, Tang T, Singapuri A, Han PL, Lopez JE, Hammond HK, Chiamvimonvat N.** Disruption of adenylyl cyclase type V does not rescue the phenotype of cardiac-specific overexpression of Galphaq protein-induced cardiomyopathy. *Am J Physiol Heart Circ Physiol* 299: H1459–H1467, 2010.
78. **Vatner DE, Sato N, Ishikawa Y, Kiuchi K, Shannon RP, Vatner SF.** Beta-adrenoceptor desensitization during the development of canine pacing-induced heart failure. *Clin Exp Pharmacol Physiol* 23: 688–692, 1996.
79. **Vatner SF, Vatner DE, Yan L.** Models of longevity (calorie restriction and AC5 KO): result of three bad hypotheses. *Aging (Albany NY)* 4: 662–663, 2012.
80. **Weiss EP, Racette SB, Villareal DT, Fontana L, Steger-May K, Schechtman KB, Klein S, Holloszy JO.** Improvements in glucose tolerance and insulin action induced by increasing energy expenditure or decreasing energy intake: a randomized controlled trial. *Am J Clin Nutr* 84: 1033–1042, 2006.
81. **Wilkins BJ, Dai YS, Bueno OF, Parsons SA, Xu J, Plank DM, Jones F, Kimball TR, Molkentin JD.** Calcineurin/NFAT coupling participates in pathological, but not physiological, cardiac hypertrophy. *Circ Res* 94: 110–118, 2004.
82. **Willoughby D, Cooper DM.** Organization and Ca^{2+} regulation of adenylyl cyclases in cAMP microdomains. *Physiol Rev* 87: 965–1010, 2007.
83. **Willoughby D, Wachten S, Masada N, Cooper DM.** Direct demonstration of discrete Ca^{2+} microdomains associated with different isoforms of adenylyl cyclase. *J Cell Sci* 123: 107–117, 2010.
84. **Yan L, Park JY, Dillinger JG, De Lorenzo MS, Yuan C, Lai L, Wang C, Ho D, Tian B, Stanley WC, Auwerx J, Vatner DE, Vatner SF.** Common mechanisms for calorie restriction and adenylyl cyclase type 5 knockout models of longevity. *Aging Cell* 11: 1110–1120, 2012.
85. **Yan L, Vatner DE, O'Connor JP, Ivessa A, Ge H, Chen W, Hirotani S, Ishikawa Y, Sadoshima J, Vatner SF.** Type 5 adenylyl cyclase disruption increases longevity and protects against stress. *Cell* 130: 247–258, 2007.
86. **Zaccolo M, Pozzan T.** Discrete microdomains with high concentration of cAMP in stimulated rat neonatal cardiac myocytes. *Science* 295: 1711–1715, 2002.
87. **Zhang G, Liu Y, Ruoho AE, Hurley JH.** Structure of the adenylyl cyclase catalytic core. *Nature* 386: 247–253, 1997.

Physical Parameters to Enhance AC Magnetically Induced Heating Power of Ferrite Nanoparticles for Hyperthermia in Nanomedicine

Minhong Jeun, Sanghoon Lee, Yu Jeong Kim, Hwa Yeon Jo, Ki Ho Park, Sun Ha Paek, Yasushi Takemura, *Member, IEEE*, and Seongtae Bae, *Member, IEEE*

***Abstract*—Solid-state ferrimagnetic MFe_2O_4 (M = Mg, Ni, Co; mean diameter size d = 30–35 nm) and superparamagnetic MFe_2O_4 (M = Mg, Ni, $Mn_{0.5}Zn_{0.5}$; d = 6–8 nm) nanoparticles [ferromagnetic nanoparticles (FMNPs) and superparamagnetic nanoparticles (SPNPs)] were used to explore the physical mechanisms of ac magnetically induced heating and identify what physical parameters would be the most critical to enhance the ac magnetically induced heating power for local *in vivo* hyperthermia agent applications. It was experimentally confirmed that "dc (minor) hysteresis loss power" generated by the magnetization reversal process, and "Néel relaxation loss power" generated by fluctuation of the magnetic moment dominantly contribute to the ac heat generation of FMNPs and SPNPs, respectively. In addition, all the experimentally and physically analyzed results demonstrated that the improvement of in-phase magnetic susceptibility χ'_m is directly relevant to the "dc (minor) hysteresis loss power" as well as the dc magnetic softness, and the out-of-phase magnetic susceptibility χ''_m is directly relevant to the "Néel relaxation loss power (or ac magnetic hysteresis loss power, A)" as well as the ac magnetic softness are the most crucial physical parameters responsible for enhancing the ac magnetically induced heating power of solid-state FMNPs and SPNPs, respectively. Particularly, some technical and engineering approaches, which can improve the χ'_m of FMNPs and the χ''_m of SPNPs, were proposed and introduced in this study to provide crucial information how to effectively design and develop a new promising hyperthermia agent in nanomedicine.**

***Index Terms*—Hysteresis loss power, magnetic nanoparticle hyperthermia, physical parameters, relaxation loss power.**

I. Introduction

LOCAL *in vivo* hyperthermia using superparamagnetic nanoparticles (SPNPs) or ferromagnetic nanoparticles (FMNPs) agents, magnetic fluid hyperthermia (MFH), has been considered to be an efficacious cancer treatment modality due to its biotechnical promises [1]–[4]. Among several kinds of nanoparticles, especially cubic spinel-structured ferrite nanoparticles have been widely studied for MFH agent applications, because they have chemically stable structures and can be molecularly engineered to provide a variety of magnetic properties by controlling their chemical compositions [5], [6]. Accordingly, a large number of primary research activities relevant to theoretical and experimental studies such as the development of various kinds of high-performance SPNPs or FMNPs agents and the development of various coating techniques of SPNPs or FMNPs agents for improving monodispersion status in ferrofluids and injection, including "intraarterial injection," and "intratumoral injection" targeting for "liver and lung cancers, etc.," and "prostate and renal cancers, etc.," respectively, have been made and are being intensively carried out for real clinical use [7]–[14]. However, despite the huge biotechnical and scientific efforts, this modality still faces critical challenges: 1) systemic "side effects"; 2) recurrence (bad prognosis); and 3) inhomogeneous heating of targeted cancer cells. One of the main physical reasons for these technical limitations is that there has been no report so far on the successful development of SPNPs or FMNPs, which can exhibit exceptionally high specific loss power (SLP) and sufficiently high enough ac magnetically induced heating temperature ($\Delta T_{ac,mag}$) as well as ultra-fast ac heating rate at the biologically and physiologically tolerable range of applied magnetic field ($H_{appl} < 190$ Oe) and frequency ($f_{appl} < 100$ kHz). Moreover, the lack of understanding on the ac magnetically induced heating mechanism of SPNPs and FMNPs, i.e., Néel or Brownian relaxation loss power $P_{relaxation\,loss}$ and hysteresis (minor hysteresis) loss power $P_{hysteresis\,loss}$, and the physical nature of ac heating characteristics such as what physical parameters dominantly contribute to the total ac heating power (P_{total}), the $P_{hysteresis\,loss}$, and $P_{relaxation\,loss}$ of SPNPs and FMNPs, is considerably responsible for the technical limitations of current MFH. Therefore, research efforts to

Manuscript received July 2, 2012; revised January 8, 2013; accepted February 10, 2013. Date of publication February 14, 2013; date of current version May 6, 2013. The review of this paper was arranged by Associate Editor G. Ramanath.

M. Jeun, S. Lee, and S. Bae are with the Biomagnetics Laboratory, Department of Electrical and Computer Engineering, National University of Singapore, Singapore 117576, Singapore (e-mail: mmhjeun@gmail.com; biomagmedic@gmail.com; elebst@nus.edu.sg).

Y. J. Kim is with the Department of Ophthalmology, Seoul National University College of Medicine, Seoul 110-744, Korea (e-mail: yjkimhappy@hanmail.net).

H.-Y. Jo is with the Department of Neurosurgery, Ischemic/Hypoxic Disease Institute, Cancer Research Institute, College of Medicine, Seoul National University, Seoul 110-744, Korea (e-mail: hyhyhy1212@naver.com).

K. H. Park is with the Department of Ophthalmology, Seoul National University College of Medicine, Seoul 110-744, Korea, and also with Seoul Artificial Eye Center, Clinical Research Institute, Seoul National University Hospital, Seoul 110-744, Korea (e-mail: kihopark@snu.ac.kr).

S. H. Paek is with Seoul National University Hospital, Jongno-gu, Seoul 110-744, Korea (e-mail: paeksh@snu.ac.kr).

Y. Takemura is with the Department of Electrical and Computer Engineering, Yokohama National University, Yokohama 240-8501, Japan (e-mail: takemura@ynu.ac.jp).

Color versions of one or more of the figures in this paper are available online at http://ieeexplore.ieee.org.

Digital Object Identifier 10.1109/TNANO.2013.2247414

systematically investigate the physical mechanism and the characteristics of ac magnetically induced heating of SPNPs and FMNPs are urgently needed to achieve highly efficient MFH modality for real clinical applications.

In this study, we explored the physical mechanism of $\Delta T_{\mathrm{ac,mag}}$ and identified what physical parameters would be the most critical to enhance the $P_{\mathrm{hysteresis\,loss}}$ and the $P_{\mathrm{relaxation\,loss}}$ of FMNPs and SPNPs using successfully synthesized solid-state ferrimagnetic MFe_2O_4 [M = Mg, Ni (soft) and Co (hard)] and superparamagnetic MFe_2O_4 (M = Mg, Ni, and $Mn_{0.5}Zn_{0.5}$) nanoparticles for local *in vivo* hyperthermia agent applications. In order to quantitatively estimate the ac heating characteristics and to build up a physical model, which can describe the real contribution of $P_{\mathrm{hysteresis\,loss}}$ and $P_{\mathrm{relaxation\,loss}}$ to the P_{total} of both FMNPs and SPNPs, intrinsic magnetic properties of FMNPs and SPNPs such as ac hysteresis loss behavior, dc (minor) hysteresis behavior, and in-phase (χ'_m) or out-of-phase (χ''_m) magnetic susceptibility were experimentally measured and analyzed. In addition, based on the experimentally analyzed results, some technical and engineering approaches, which can improve the χ'_m of FMNPs and the χ''_m of SPNPs, were proposed and introduced to provide crucial information how to effectively design and develop a new promising hyperthermia agent.

II. Experiment

FMNPs and SPNPs were synthesized by sol-gel, and high-temperature thermal decomposition (HTTD) methods, respectively. The size and the size distribution of the synthesized nanoparticles were determined using a field emission scanning electron microscopy (FE-SEM) and a high-resolution transmission electron microscopy (HR-TEM). The $\Delta T_{\mathrm{ac,mag}}$ characteristics and the ac hysteresis loss behavior were measured by using a specially designed ac solenoid coil–capacitor system. For measuring the self-heating temperature rise of the nanoparticles, they were put in a microcentrifuge tube and an optical thermometer was inserted into the nanoparticles. The f_{appl} and the H_{appl} during $\Delta T_{\mathrm{ac,mag}}$ and ac hysteresis loop measurement were fixed at 110 kHz and 140 Oe, respectively. The dc minor hysteresis loop and the initial magnetization curve were measured by using a vibrating sample magnetometer (VSM), and a physical property measurement system (PPMS) was employed to determine the χ'_m and χ''_m of the synthesized nanoparticles. The contribution of $P_{\mathrm{hysteresis\,loss}}$ and $P_{\mathrm{relaxation\,loss}}$ to the P_{total} of FMNPs and SPNPs were quantitatively analyzed based on the experimentally obtained results including $\Delta T_{\mathrm{ac,mag}}$, ac and dc magnetic minor hysteresis loops, and magnetic susceptibilities. The cytotoxicity and the cellular uptake of the synthesized nanoparticles were investigated by employing methyl thiazol tetrazolium (MTT) bromide test and a TEM using neuronal stem cells isolated from human fetal midbrain, human neural cells, and normal mouse liver cells to evaluate the biocompatibility and to investigate the biofeasibility to hyperthermia agent applications.

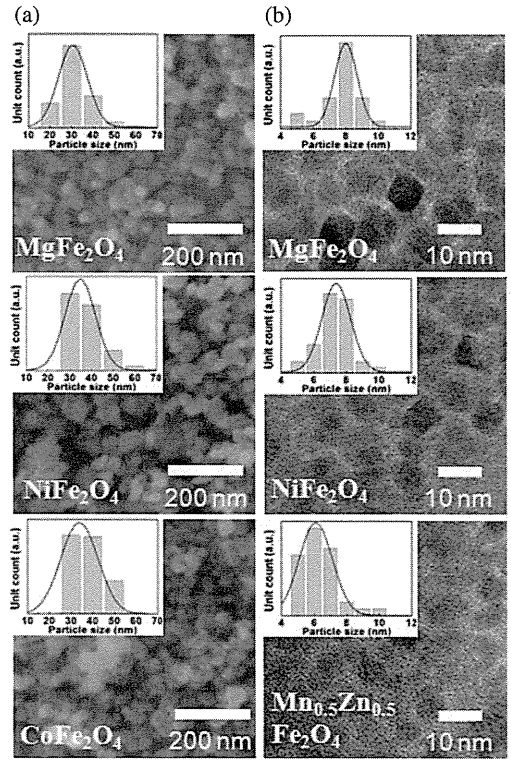

Fig. 1. The particle size and the size distributions of the synthesized (a) ferrimagnetic $MgFe_2O_4$, $NiFe_2O_4$, and $CoFe_2O_4$ nanoparticles and (b) superparamagnetic $MgFe_2O_4$, $NiFe_2O_4$, and $Mn_{0.5}Zn_{0.5}Fe_2O_4$ nanoparticles measured by FE-SEM and HR-TEM, respectively.

III. Results and Discussion

A. Structural, magnetic, and ac magnetically induced heating properties of ferrite ferrimagnetic and superparamagnetic nanoparticles

FE-SEM and HR-TEM images [see Fig. 1(a) and (b)] show the size and the size distribution of the nanoparticles synthesized by (a) sol–gel and (b) HTTD methods. The nanoparticles shown in Fig. 1(a) had a mean particle diameter d of 30–35 nm with a 27% standard deviation, and the nanoparticles shown in Fig. 1(b) had d = 6–8 nm with a 12.5% standard deviation. In order to verify the ferrimagnetic and superparamagnetic nature of the synthesized nanoparticles, dc minor hysteresis behavior of the nanoparticles was investigated at the sweeping field H_{appl} of $\pm$140 Oe at room temperature (RT). As can be seen in Fig. 2(a), the $MgFe_2O_4$and $NiFe_2O_4$ nanoparticles with d = 30–35 nm had dc minor hysteresis loss, indicating that they are ferrimagnetic nanoparticles. However, although the $CoFe_2O_4$nanoparticles with d = 35 nm showed a large hysteresis loss at the sweeping field H_{appl} of $\pm$15 kOe, they had almost zero dc minor hysteresis loss with very small magnetization value at the H_{appl} of $\pm$140 Oe. This is mainly though to be due to their high magnetic anisotropy [15]. Fig. 2(b) shows the dc minor hysteresis behavior of the nanoparticles synthesized by using HTTD method. The nanoparticles did not exhibit any dc minor hysteresis loss directly, indicating that these nanoparticles are superparamagnetic nanoparticles.

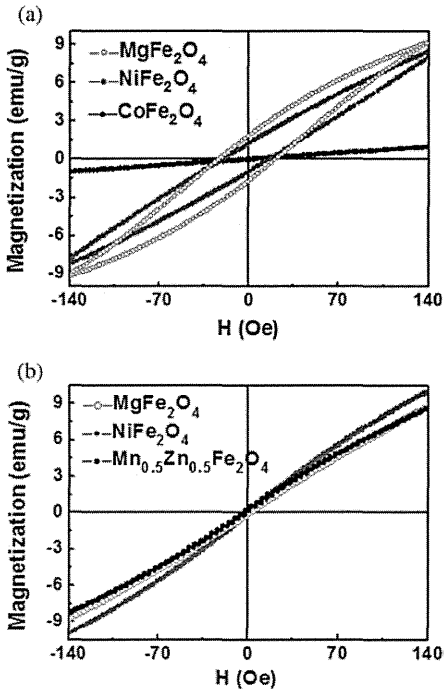

Fig. 2. DC minor hysteresis loop of (a) ferrimagnetic nanoparticles and (b) superparamagnetic nanoparticles measured at a dc H_{appl} of $\pm$140 Oe.

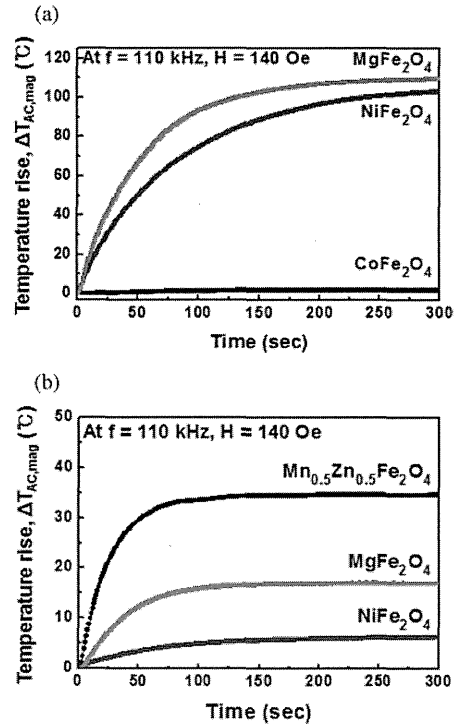

Fig. 3. AC magnetically induced heating temperatures of solid-state (a) ferrimagnetic nanoparticles and (b) superparamagnetic nanoparticles measured at the fixed H_{appl} of 140 Oe and f_{appl} of 110 kHz.

In order to investigate the ac magnetically induced heating characteristics of all the nanoparticles shown in Fig. 1, the $\Delta T_{\mathrm{ac,mag}}$ was measured at the fixed f_{appl} of 110 kHz and H_{appl} of 140 Oe. Fig. 3(a) and (b) shows the $\Delta T_{\mathrm{ac,mag}}$ of the FMNPs and SPNPs, respectively. The $MgFe_2O_4$ FMNPs exhibited the highest $\Delta T_{\mathrm{ac,mag}}$ and the $CoFe_2O_4$ FMNPs had the lowest $\Delta T_{\mathrm{ac,mag}}$, whereas for the case of SPNPs, the $Mn_{0.5}Zn_{0.5}Fe_2O_4$ SPNPs exhibited the highest $\Delta T_{\mathrm{ac,mag}}$ and the $NiFe_2O_4$ SPNPs had the lowest $\Delta T_{\mathrm{ac,mag}}$. In order to systematically understand the ac heating characteristics and to identify the physical parameters, which can potentially improve the $\Delta T_{\mathrm{ac,mag}}$ of FMNPs and SPNPs, the intrinsic magnetic properties, i.e., initial magnetic susceptibility (initial χ_m), χ'_m, χ''_m, dc minor hysteresis behavior, and ac hysteresis loop characteristics of the FMNPs and SPNPs were experimentally investigated. In addition, the physical contribution of $P_{\mathrm{hystersis\,loss}}$ and $P_{\mathrm{relaxation\,loss}}$ to the P_{total} was calculated and analyzed based on the experimentally measured results to explore the physical nature of ac heating mechanism in both FMNPs and SPNPs.

B. Physical Mechanism and Parameters of AC Magnetically Induced Heating Power of Ferrite Ferrimagnetic Nanoparticles

The $P_{\mathrm{hystersis\,loss}}$ given by (1) is defined as the ac magnetically induced heat generation per unit volume of magnetic nanoparticles given by the f_{appl} multiplied by the area of dc minor hysteresis loss. The $P_{\mathrm{hystersis\,loss}}$ is generally induced by the lagging of magnetic moment at a constant ac magnetic field that is why it is closely related to the physical nature of ac heat generation of ferrimagnetic or ferromagnetic nanoparticles, whereas the $P_{\mathrm{relaxation\,loss}}$ is defined as the ac magnetically induced heat generation caused by either spin relaxation (or rotation), "Néel relaxation," in a core of magnetic nanoparticle or magnetomechanical friction force generated among the rotating magnetic nanoparticles due to the increase of surrounding temperature and the change of (bio)chemical environment, "Brown relaxation". The $P_{\mathrm{relaxation\,loss}}$ dominantly contributes to the ac heating power of SPNPs, because they have no dc minor hysteresis loss. In addition, the $P_{\mathrm{relaxation}}$ is directly proportional to the χ''_m of SPNPs expressed as a function of the Néel relaxation (τ_N) or Brown relaxation (τ_B) [see (2) and (3)]. However, for the solid-state SPNPs with $d = 6$–8 nm considered in this study, it can be assumed that: 1) τ_N is much faster than τ_B; 2) τ_B can be negligible due to relatively high packing fraction; and 3) τ_B can be neglected, because it is hard to define the viscosity η [$\tau_B = 3\eta V_H/k_BT, V_H$: hydrodynamic volume, $\therefore \tau \cong \tau_N$ in (2)] [18]. Therefore, the $P_{\mathrm{relaxation\,loss}}$ of solid-state SPNPs can be simply assumed to be $P_{\mathrm{Neel\,relaxation\,loss}}$, as expressed by (3):

$$P_{\mathrm{hysteresis\,loss}} = \mu_0 f_{\mathrm{appl}} \int H_{\mathrm{dc,appl}} \cdot dM \tag{1}$$

$$\chi''_m = \chi_0 \frac{2\pi f\tau}{1+(2\pi f\tau)^2} \quad \left(\frac{1}{\tau} = \frac{1}{\tau_N} + \frac{1}{\tau_B} \cong \frac{1}{\tau_N}\right) \tag{2}$$

$$P_{\mathrm{relaxation\,loss}} \cong P_{\mathrm{Neel\,relaxation\,loss}} = \pi\mu_0 \chi''_m f_{\mathrm{appl}} H^2_{\mathrm{ac,appl}}. \tag{3}$$

Considering (1), the main physical reason for obtaining the highest $\Delta T_{\mathrm{ac,mag}}$ (or $P_{\mathrm{hystersis\,loss}}$; see Table I) of $MgFe_2O_4$ FMNP can be thought to be due to the largest dc minor hysteresis power resulted from the highest dc magnetic softness. The higher dc magnetic softness leads to a faster response of magnetic spins

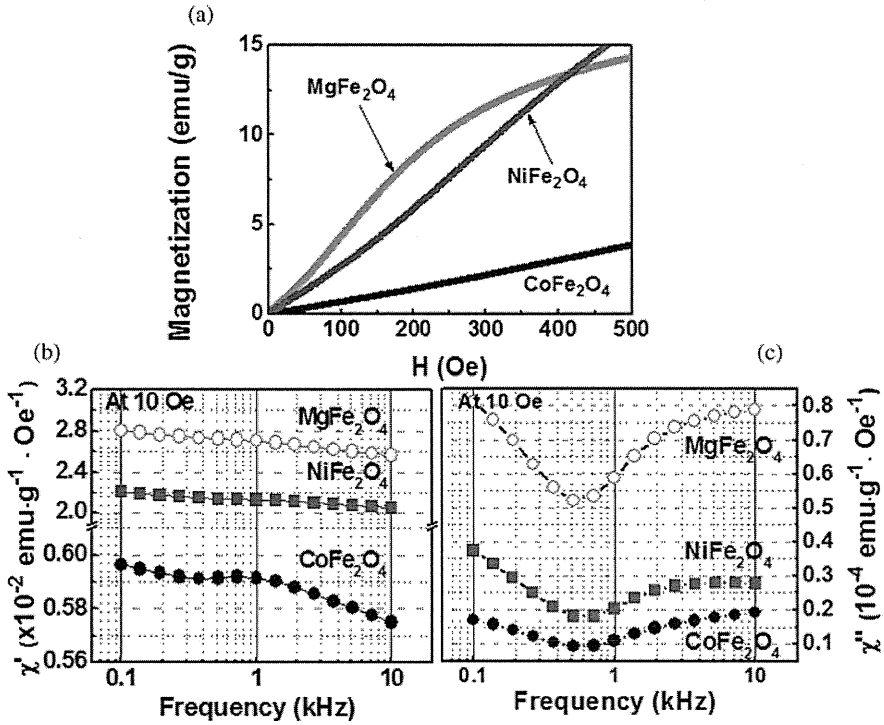

Fig. 4. Intrinsic magnetic properties of all the three ferrimagnetic nanoparticles shown in Fig. 1(a): (a) initial $M - H$ curve, (b) in-phase magnetic susceptibility, and (c) out-of-phase magnetic susceptibility.

TABLE I
CALCULATION RESULTS OF THE REAL CONTRIBUTIONS OF $P_{\text{hystersis loss}}$ [(a) FERRIMAGNETIC NANOPARTICLES] AND $P_{\text{Neel relaxation loss}}$ [(b) SUPERPARAMAGNETIC NANOPARTICLES] TO THE P_{total} AND THE MAGNETIC ANISOTROPY VALUE OF EACH SUPERPARAMAGNETIC NANOPARTICLES

(a)

Nanoparticle	Hysteresis loss energy (erg/cm³)	$P_{\text{hysteresis loss}}$ (W/m³)	$P_{\text{Neel relaxation loss}}$ (W/m³)	P_{total} (W/m³)	$P_{\text{hysteresis loss}}$ (%)
$MgFe_2O_4$	2898	3.19×10^7	1.04×10^6	3.28×10^7	~97
$NiFe_2O_4$	2246	2.45×10^7	8.33×10^5	2.53×10^7	~97
$CoFe_2O_4$	37.26	4.1×10^5	1.93×10^5	5.99×10^5	~68

(b)

Nanoparticle	Anisotropy constant (erg/cm³)	$P_{\text{Neel relaxation loss}}$ (W/m³)	P_{total} (W/m³)	$P_{\text{Neel relaxation loss}}$ (%)
$MgFe_2O_4$	-0.4×10^5	4.96×10^6	5.1×10^6	97.2
$NiFe_2O_4$	-0.7×10^5	1.40×10^6	1.49×10^6	93.9
$Mn_{0.5}Zn_{0.5}Fe_2O_4$	-0.18×10^5	6.54×10^6	6.77×10^6	96.6

to the externally applied magnetic field due to a larger magnetic exchange energy (or lower magnetic anisotropy) resulting in a higher initial χ_m as well as χ'_m. Accordingly, it generates a larger dc magnetization value ($M = \chi_m \mathrm{H}$, $\chi_m = \chi'_m + i\chi''_m$) as well as a larger dc minor hysteresis loss or loss power $P_{\text{hystersis loss}}$. In order to experimentally verify this physical assumption, χ'_m, χ''_m, the initial χ_m, and the dc minor hysteresis behavior of all the three FMNPs shown in Fig. 1 were investigated and compared. As shown in Figs. 2 and 4, the $MgFe_2O_4$ FMNPs showed the highest initial χ_m and χ'_m values and correspondingly the largest dc minor hysteresis loss as well as the highest $\Delta T_{\text{ac,mag}}$. In contrast, the $CoFe_2O_4$ FMNPs showed the lowest initial χ_m and χ'_m values and accordingly almost zero dc minor hysteresis as well as the lowest $\Delta T_{\text{ac,mag}}$. All the experimentally confirmed results shown in Figs. 2–4 indicate that the physical nature (mechanism) of ac magnetically induced heating power of FMNPs are closely related to the dc minor hysteresis loss (or loss power $P_{\text{hystersis loss}}$), which is directly affected by the dc magnetic softness (or magnetic exchange coupling). However, it was interestingly found that the FMNPs had extremely small χ''_m values and there is no physical relationship between the $\Delta T_{\text{ac,mag}}$ and the χ''_m in ac heating characteristics [Fig. 4(c)].

In order to quantitatively identify further how much the $P_{\text{hysteresis loss}}$ contribute to the P_{total} of FMNPs, the $P_{\text{hysteresis loss}}$ and the $P_{\text{Neel relaxation loss}}$ were numerically calculated and analyzed based on the experimentally measured results. The P_{total} was determined from the following equation:

$$P_{\text{total}} = C_{\text{vol}} m T_{\max} \tag{4}$$

where C_{vol} is the volumetric heat capacity, m the mass of nanoparticles, and $T_{\max}$ is the maximum ac heating temperature. As can be seen in Table I, the $MgFe_2O_4$ ($\Delta T_{\text{ac,mag}} = 110\ ^\circ\text{C}$) and $NiFe_2O_4$ ($\Delta T_{\text{ac,mag}} = 102\ ^\circ\text{C}$) FMNPs with higher dc magnetic softness (or higher magnetic exchange, or lower magnetic anisotropy) and correspondingly higher initial χ_m and χ'_m values showed large hysteresis loss energy or hysteresis loss power $P_{\text{hystersis loss}}$ at the ac sweeping field of ± 140 Oe. These two values are 60–77 times larger than that of the $CoFe_2O_4$ FMNPs ($\Delta T_{\text{ac,mag}} = 2\ ^\circ\text{C}$). In particular, Table I shows that ~97%

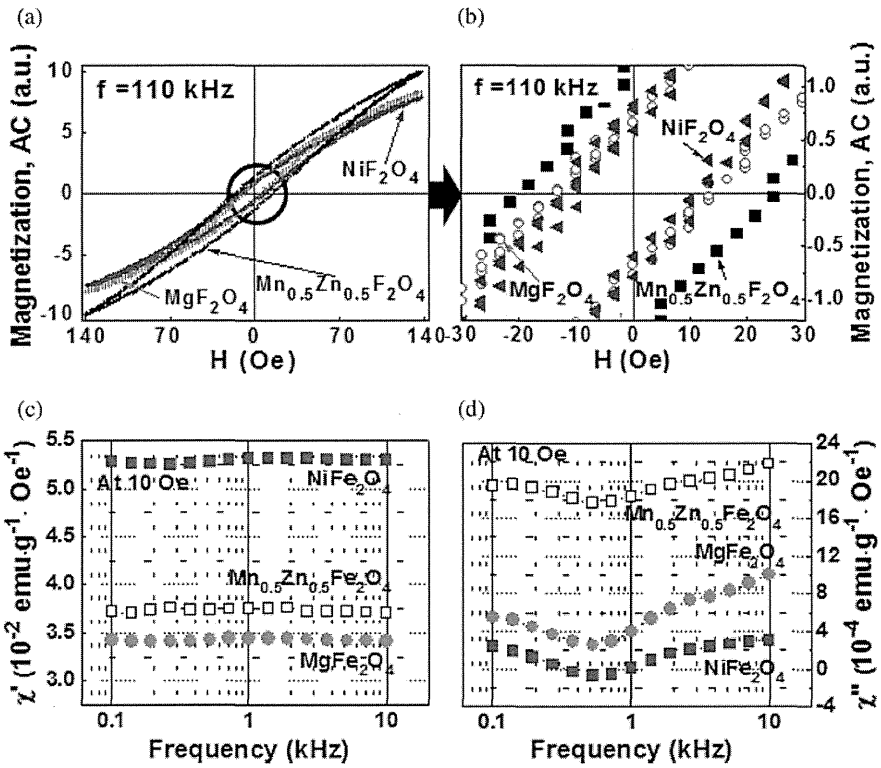

Fig. 5. Intrinsic magnetic properties of all the three superparamagnetic nanoparticles shown in Fig. 1(b): (a) ac hysteresis loop, (b) ac hysteresis loop measured at the sweeping field of ±25 Oe with $f_{\rm appl}$: 110 kHz, (c) in-phase magnetic susceptibility, and (d) out-of-phase magnetic susceptibility.

of $P_{\rm hystersis\,loss}$ contribute to the $P_{\rm total}$ of soft $MgFe_2O_4$ and $NiFe_2O_4$ FMNPs. These results strongly support the physical fact that the dc (minor) hysteresis loss power plays a dominant role in determining the $\Delta T_{\rm ac,mag}$ and the ac magnetically induced heating characteristics of FMNPs.

According to all the results shown in Figs. 2–4, it can be conclusively summarized that χ'_m is the most crucial physical parameter to improve the $P_{\rm hystersis\,loss}$ and correspondingly the $\Delta T_{\rm ac,mag}$ of FMNPs. Therefore, the enhancement of χ'_m would be a dominantly key factor for achieving a promising FMNP hyperthermia agent in nanomedicine. The technical approaches, which can tailor the magnetic anisotropy and the magnetic exchange coupling of FMNPs, such as: 1) controlling the composition/distribution of cations in FMNPs during synthesis, and 2) modifying the particle dipole–dipole interaction by changing the size, the size distribution, or the shape of FMNPs, can be considerably suggested to physically improve the χ'_m of FMNPs for hyperthermia agent applications [15]–[17].

C. Physical Mechanism and Parameters of AC Magnetically Induced Heating Power of Ferrite Superparamagnetic Nanoparticles

The physical mechanism of ac heating characteristics of SPNPs could be differently understood, because SPNPs did not exhibit any dc minor hysteresis loss [see Fig. 2(a)] and any physical dependence on χ'_m [see Fig. 5(c)]. Accordingly, we explored the physical relationship between the intrinsic ac magnetic properties such as ac hysteresis loss or area ($\mathscr{A}$) and χ''_m, and the ac magnetically induced heating characteristics of SPNSs to identify what physical mechanism is dominant and what physical parameters are crucial to significantly improve the ac heating power of SPNPs for hyperthermia agent applications. The χ''_m and $\mathscr{A}$ are induced by the response of magnetic spins (moments) to the externally applied ac magnetic field. Hence, their physical relationship can be described and expressed by (5)–(8).

The magnetization of SPNPs under ac magnetic field can be expressed by

$$M_{(\omega t)} = \chi''_m B_{\rm ac,appl} \quad (B_{\rm ac,appl}\text{is the total flux density } (\mu H_{\rm ac,appl})) \tag{5}$$

where χ''_m is defined as [19]

$$\chi''_m = \frac{1}{\pi B_{\rm ac,appl}} \int_0^{2\pi} M(\omega t)\sin(\omega t) d(\omega t) \tag{6}$$

and $\mathscr{A}$ is defined as [20]

$$\mathscr{A} = \int_0^{2\pi} M(\omega t)\sin(\omega t) d(\omega t). \tag{7}$$

Therefore, the physical relationship between χ''_m and $\mathscr{A}$ can be expressed as follows:

$$\chi''_m = \frac{1}{\pi\mu H_{\rm ac,appl}} \mathscr{A}. \tag{8}$$

In addition, by substituting (8) into (3), the $P_{\rm Neel\,relaxation\,loss}$ can be rewritten as (9). According to (9) and (8), it can be

clearly understood that $P_{\text{Neel relaxation loss}}$ of SPNPs under ac magnetic field is the same as the ac hysteresis loss power $P_{\text{ac hysteresis loss}}$. In particular, it is physically confirmed that: 1) $P_{\text{Neel relaxation loss}}$ and $P_{\text{ac hysteresis loss}}$ are directly proportional to $\mathscr{A}$; and 2) $\mathscr{A}$ is directly proportional to χ_m'':

$$P_{\text{Neel relaxation loss}} = P_{\text{ac hysteresis loss}} = f_{\text{appl}} H_{\text{ac,appl}}\, \mathscr{A}/\mu_r$$
$$\mu_r : \text{relative permeability.} \tag{9}$$

As described in (5)–(9), $P_{\text{Neel relaxation loss}}$ is the main physical mechanism responsible for the ac heating power of SPNPs and its contribution to P_{total} of SPNPs can be directly estimated by experimentally evaluating both χ_m'' and $\mathscr{A}$. Hence, χ_m'' and $\mathscr{A}$ of all the three SPNPs used in this study were measured and compared to confirm the physical relation and the role in characterizing the ac heating properties of SPNPs. Fig. 5 shows the ac magnetic properties of SPNPs including ac magnetic hysteresis behavior measured at $f_{\text{appl}} = 110$ kHz and $H_{\text{ac,appl}} = \pm 140$ Oe and the ac magnetic susceptibility (χ_m' and χ_m'') measured at the activation magnetic field of 10 Oe under the ac frequency varied from 100 Hz to 10 kHz. In addition, Table I(b) summarizes the calculated $P_{\text{Neel relaxation loss}}$, P_{total}, $P_{\text{Neel relaxation loss}}/P_{\text{total}}$, and magnetic anisotropy of all the three SPNPs ($Mn_{0.5}Zn_{0.5}Fe_2O_4$, $MgFe_2O_4$, and $NiFe_2O_4$) based on the experimentally measured results. Among the three SPNPs, the $Mn_{0.5}Zn_{0.5}Fe_2O_4$ SPNPs, which showed the largest $P_{\text{Neel relaxation loss}}$ and P_{total} with a $P_{\text{Neel relaxation loss}}/P_{\text{total}}$ of 96.6%, had the largest $\mathscr{A}$ (highest ac magnetic softness) and χ_m''. In contrast, the $NiFe_2O_4$ SPNPs, which showed the smallest $P_{\text{Neel relaxation loss}}$ and P_{total} with a $P_{\text{Neel relaxation loss}}/P_{\text{total}}$ of 93.9%, had the smallest $\mathscr{A}$ (lowest ac magnetic softness) and χ_m''. These experimentally and quantitatively analyzed results shown in Fig. 5 and Table I(b) demonstrate that $P_{\text{Neel relaxation loss}}$ dominantly contributes to the P_{total} of SPNPs and it is directly proportional to $\mathscr{A}$ [see (9)] as well as χ_m''. In particular, these results provide us crucial information that the ac heating ability of SPNPs can be directly estimated by measuring the ac hysteresis behavior or the ac hysteresis loss (area) at the same ac magnetic field condition of ac magnetically induced heating because χ_m'', which is related to the "Néel relaxation of magnetic spins τ_N" [see (2)], is directly proportional to the $\mathscr{A}$ [see (8)]. In order to more clearly understand the physical relationship between $\mathscr{A}$ and χ_m'' as well as their effects on the ac heat generation of SPNPs, magnetic anisotropy (K) of the SPNPs and the physical correlation with $\mathscr{A}$ and χ_m'' were explored. The main reason for this study is that K is closely relevant to the magnetic spin motion (relaxation) or "Néel relaxation of magnetic spins τ_N" and χ_m'', as described in (10) [17] and (2), respectively:

$$\tau_N = \tau_0 \exp\left(\frac{KV}{k_B T}\right) \tag{10}$$

where τ_0 is the relaxation time constant, V the volume of particle, k_B the Boltzmann constant, and T the temperature.

In addition, the relationship among $\mathscr{A}$, χ_m'', and K can be clearly expressed by combining (2), (8), and (10) as follows:

$$\mathscr{A} = \chi_m'' \pi \mu H_{\text{ac,appl}}, \left(\chi'' \propto \frac{1}{\tau_N} \propto \frac{1}{K}\right), \quad \mathscr{A} \propto \frac{1}{K}. \tag{11}$$

According to (11), it can be physically understood that $\mathscr{A}$ and χ_m'' are inversely proportional to the K of SPNPs. As experimentally confirmed in Table I(b), the $Mn_{0.5}Zn_{0.5}Fe_2O_4$ SPNPs, which showed the largest $\mathscr{A}$, exhibited the lowest K value (highest ac magnetic softness), while the $NiFe_2O_4$ SPNPs, which showed the smallest $\mathscr{A}$, had the highest K (lowest ac magnetic softness). These results indicate that the significant enhancement of $\mathscr{A}$ (or χ_m'') by controlling the ac magnetic softness (K, or magnetic exchange coupling) is the most important physical parameter (or approach) to improve the P_{total} ($P_{\text{Neel relaxation loss}}$) of SPNPs for MFH agent applications in nanomedicine. The ac magnetic softness of SPNPs such as ferrite SPNPs, MFe_2O_4 (M: transition metals) SPNPs, could be enhanced by improving the exchange energy (coupling), the ac frequency response, and the τ_N. The addition of a nonmagnetic cation to the tetrahedral site or the addition of a magnetic cation, which has a higher Bohr magneton than that of iron, to the octahedral site of ferrite SPNPs could be introduced and proposed as a critical approach to improve the magnetic exchange coupling or to reduce the magnetic anisotropy. In addition, shallow doping of a new cation with a faster τ_0 such as cobalt ion or substitution of cation with higher magnetic permeability by tetrahedral site of ferrite SPNPs would be proposed to improve the ac frequency response time and spin relaxation time [21]–[24].

D. Biocompatibility of Ferrite Ferrimagnetic and Superparamagnetic Nanoparticles

In addition to the studies on the ac magnetically induced heating characteristics and the physical nature of ac heating mechanism of ferrite FMNPs and SPNPs, in order to evaluate the feasibility of FMNPs and SPNPs used in this study to a local hyperthermia agent, the *in vitro* biocompatibility (or cytotoxicity) of the nanoparticles were investigated by employing MTT and TEM studies with normal rat liver epidermal cells (for FMNPs) and neuronal stem cells isolated from human fetal midbrain (for SPNPs). Fig. 6 shows the cell survival rate of (a) the FMNPs and (b) the SPNPs under different nanoparticle concentrations. As can be seen in Fig. 6(a) and (b), the FMNPs showed a high cell survival rates of 90%–80% (noncytotoxicity) and the SPNPs showed cell survival rates of 87%–65% (non- or midcytotoxicity) with standard deviations of 8%–10% depending on the nanoparticle concentrations. The studies on the uptake characteristic of the SPNPs by a cell and its cytological change caused by the infused SPNPs were conducted by TEM using human neural cells (F3Lacz). In order to necrotize cancer cells, the nanoparticle agents have to be initially absorbed by the cells and located inside the cells without side effects such as cell deformation, inflammation, and nucleus fragmentation. As can be seen in Fig. 6(c), all the SPNPs were successfully uptake and located in the cytoplasm of F3Lacz (black arrows) without any side effects. The relatively high biocompatibility

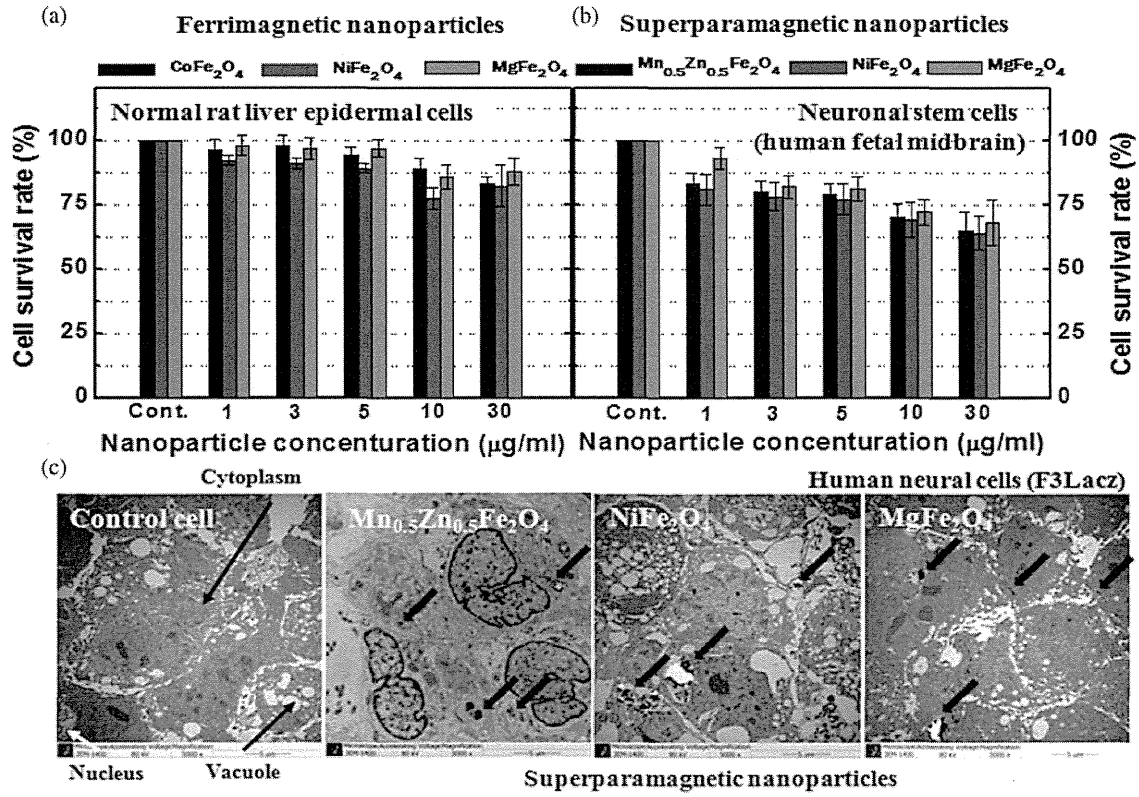

Fig. 6. Studies of *in vitro* biocompatibility of the ferrimagnetic and superparamagnetic nanoparticles: (a) cell survival rate of all the ferrimagnetic nanoparticles with normal rat liver epidermal cells, (b) cell survival rate of all the superparamagnetic nanoparticles with neuronal stem cells, and (c) TEM study results of cellular uptake characteristics of all the superparamagnetic nanoparticles by human neural cells.

of all the FMNPs and SPNPs used in this study demonstrated that they can be potentially considered to be an *in vivo* hyperthermia agent. However, ideally, considering the clearance of nanoparticles by the reticuloendothelial system (RES) and the blood clotting problem caused by aggregated nanoparticles, SPNPs in the range of 12–15 nm in diameter (core + coating layer) are considered to be more appropriate nanoparticles for *in vivo* hyperthermia agent applications.

IV. Conclusion

Solid-state MFe_2O_4 (M = Mg, Ni, Co) FMNPs and MFe_2O_4 (M = Mg, Ni, $Mn_{0.5}Zn_{0.5}$,) SPNPs were used to explore the physical mechanisms of ac magnetically induced heating and identify what physical parameters would be the most critical to enhance the ac heating power for local *in vivo* hyperthermia agent applications. According to the experimental results, $P_{\text{hysteresis loss}}$ and $P_{\text{Neel relaxation loss}}$ (or $P_{\text{ac hysteresis loss}}$) dominantly contributed to the P_{total} of FMNPs and SPNPs, respectively. Moreover, it was physically demonstrated that the initial χ_m and χ'_m, directly relevant to the dc magnetic softness, and $\mathscr{A}$ (or χ''_m), directly relevant to the ac magnetic softness, are the most crucial physical parameters to enhance the $P_{\text{hysteresis loss}}$ (FMNPs) and $P_{\text{Neel relaxation loss}}$ (SPNPs), respectively. Controlling the magnetic anisotropy, the exchange coupling (energy), and the relaxation time constant of FMNPs or SPNPs by tailoring the magnetic and structural properties of FMNPs and SPNPs would be the most efficient technical approach to significantly improve the physical parameters for their hyperthermia agent applications.

References

[1] R. K. Gilchrist, R. Medal, W. D. Shorey, R. C. Hanselman, J. C. Parrott, and C. B. Taylor, "Selective inductive heating of lymph nodes," *Ann. Surg.*, vol. 146, pp. 596–606, 1957.

[2] A. Jordan, P. Wust, R. Scholz, B. Tesche, H. Fahling, T. Mitrovics, T. Vogl, J. Cervos-Navarro, and R. Felix, "Cellular uptake of magnetic fluid particles and their effects on hyman adenocarcinima cells exposed to AC magnetic field in vitro," *Int. J. Hyperther.*, vol. 12, pp. 705–722, 1996.

[3] O. S. Neilsen, M. Horsman, and J. Overgaard, "A future for hyperthermia in cancer treatment?," *Eur. J. Cancer*, vol. 37, pp. 1587–1589, 2001.

[4] Q. A. Pankhurst, N. T. K. Thanh, S. K. Jones, and J. Dobson, "Progress in applications of magnetic nanoparticles in biomedicine," *J. Phys. D, Appl. Phys.*, vol. 42, pp. 224001–224015, 2009.

[5] S. Sun, H. Zeng, D. B. Robinson, S. Raoux, P. M. Rice, S. X. Wang, and G. Li, "Monodisperse MFe_2O_4 (M= Fe, Co, Mn) nanoparticles," *J. Amer. Chem. Soc.*, vol. 126, pp. 273–279, 2004.

[6] R. Hergt, S. Dutz, R. Müller, and M. Zeisberger, "Magnetic particle hyperthermia: Nanoparticle magnetism and materials development for cancer therapy," *J. Phys., Condens. Matter*, vol. 18, pp. S2919–S2934, 2006.

[7] J. Williams, R. Lansdown, R. Sweitzer, M. Romanowski, R. LaBell, R. Ramaswami, and E. Unger, "Nanoparticle drug delivery system for intravenous delivery of topoisomerase inhibitors," *J. Cont. Release*, vol. 91, pp. 167–172, 2003.

[8] R. M. Schiffelers, A. Ansari, J. Xu, Q. Zhou, Q. Tang, G. Storm, G. Molema, R. Y. Lu, P. V. Scaria, and M. C. Woodle, "Cancer siRNA therapy by tumor selective delivery with ligand-targeted sterically stabilized nanoparticle," *Nucl. Acids Res.*, vol. 32, pp. e149–e158, 2004.

[9] S. Mornet, S. Vasseur, F. Grasset, and E. J. Duguet, "Magnetic nanoparticle design for medical diagnosis and therapy," *J. Mater. Chem.*, vol. 14, pp. 2161–2175, 2004.
[10] M. Johannsen, U. Gneveckow, L. Eckelt, A. Feussner, N. WaldÖFner, R. Scholz, S. Deger, P. Wust, S. A. Loening, and A. Jordan, "Clinical hyperthermia of prostate cancer using magnetic nanoparticles: Presentation of a new interstitial technique," *Int. J. Hyperther.*, vol. 21, pp. 637–647, 2005.
[11] P. Bruners, T. Braunschweig, M. Hodenius, H. Pietsch, T. Penzkofer, M. Baumann, R. W. Günther, T. Schmitz-R, and H. A. Mahnken, "Thermoablation of malignant kidney tumors using magnetic nanoparticles: An in vivo feasibility study in a rabbit modal," *Cardiovasc. Interv. Radiol*, vol. 33, pp. 127–134, 2010.
[12] P. Moroz, S. K. Jones, and B. N. Gray, "Status of hyperthermia in the treatment of advanced liver cancer," *J. Surg. Oncol.*, vol. 77, pp. 252–269, 2001.
[13] P. Moroz, C. Metcalf, and B. N. Gray, "Histologic analysis of liver tissue following hepatic arterial infusion of ferromagnetic particles in a rabbit tumor model," *BioMetals*, vol. 16, pp. 455–464, 2003.
[14] M. S. Seehra, V. Singh, P. Dutta, S. Neeleshwar, Y. Y. Chen, C. L. Chen, S. W. Shou, and C. C. Chen, "Size-dependent magnetic parameters of fcc FePt nanoparticles: Applications to magnetic hyperthermia," *J. Phys. D, Appl. Phys.*, vol. 43, pp. 145002–145008, 2010.
[15] M. Jeun, S. Bae, A. Tomitaka, Y. Takemura, K. H. Park, S. H. Paek, and K. W. Chung, "Effects of particle dipole interaction on the ac magnetically induced heating characteristics of ferrite nanoparticles for hyperthermia," *Appl. Phys. Lett.*, vol. 95, pp. 082501–082504, 2009.
[16] R. E. Rosensweig, "Heating magnetic fluid with alternating magnetic field," *J. Magn. Mater.*, vol. 252, pp. 370–374, 2002.
[17] R. Hergt, S. Dutz, and M. Röder, "Effects of size distribution on hysteresis losses of magnetic nanoparticles for hyperthermia," *J. Phys., Condens. Matter.*, vol. 20, pp. 385214–385225, 2008.
[18] J. P. Fortin, C. Wilhelm, J. Servais, C. Ménager, J. C. Bacri, and F. Gazeau, "Size-sorted anionic iron oxide nanomagnets as colloidal mediators for magnetic hyperthermia," *J. Amer. Chem. Soc.*, vol. 129, pp. 2628–2635, 2007.
[19] M. I. Youssif, A. A. Bahgat, and I. A. Ali, "AC magnetic susceptibility technique for the characterization of high temperature superconductors," *Egypt. J. Sol.*, vol. 23, pp. 231–250, 2000.
[20] Y. L. Raikher, V. I. Stepanov, and R. Perzynski, "Dynamic hysteresis of a superparamagnetic nanoparticles," *Physica B*, vol. 343, pp. 262–266, 2004.
[21] B. D. Cullity, *Introduction to Magnetic Materials*. Reading, MA, USA: Addison-Wesley, 1972.
[22] A. Goldman, *Modern Ferrite Technology*. New York, NY, USA: Springer, 2006.
[23] M. Jeun, S. Moon, H. Kobayashi, H. Y. Shin, A. Tomitaka, Y. J. Kim, Y. Takemura, S. H. Paek, K. H. Park, K. W. Chung, and S. Bae, "Effects of Mn concentration on the ac magnetically induced heating characteristics of superparamagnetic $Mn_xZn_{1-x}Fe_2O_4$ nanoparticles for hyperthermia," *Appl. Phys. Lett.*, vol. 96, pp. 202511–202513, 2010.
[24] A. J. Rondinone, A. C. S. Samia, and Z. J. Zhang, "Characterizing the magnetic anisotropy constant of spinel cobalt ferrite nanoparticles," *Appl. Phys. Lett.*, vol. 76, pp. 3624–3626, 2000.

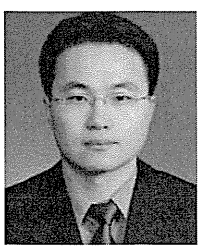

Minhong Jeun received the B.S. and M.S. degrees in electronic materials engineering from Kwangwoon University, Seoul, Korea, in 2002 and 2004, respectively. He is currently working toward the Ph.D. degree from the Department of Electrical and Computer Engineering, National University of Singapore (NUS), Singapore.

He was a Student Researcher at the Korea Institute of Science and Technology (KIST). His current research interests include the development of superparamagnetic nanoparticles for MFH agents and their applications in nanomedicine such as local induction of heat shock proteins for ocular neuroprotection and cancer theragnosis modalities.

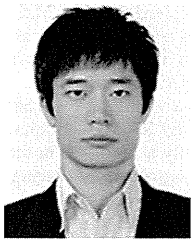

Sanghoon Lee received the B.S. degree from the Department of Electronic Material Engineering, Kwangwoon University, Seoul, Korea, in 2009. He is currently working toward the M.S. degree from the Department of Electrical and Computer Engineering, National University of Singapore (NUS), Singapore.

He is currently a Research Engineer in the Department of Electrical and Computer Engineering, NUS. His current research interests include the development of new functional superparamagentic nanoparticles and the applications to various cancer treatment/diagnosis modalities in nanomedicine.

Yu Jeong Kim received the M.S. degree in ophthalmology from Seoul National University, Seoul, Korea, in 2007.

She is currently a Researcher in the Ophthalmology Lab, Seoul National University Hospital, Seoul. Her current research interests include neuroprotection of the glaucoma model.

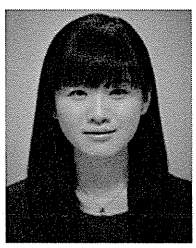

Hwa Yeon Jo received the B.S. degree in biology from Konkuk University, Seoul, Korea, in 2010. She is currently toward the Postgraduate degree in cancer biology from the Cancer Research Institute, College of Medicine, Seoul National University, Seoul, Korea.

Ki Ho Park received the M.D. and Ph.D. degrees from Seoul National University College of Medicine, Seoul, Korea.

He was a Research Fellow (glaucoma) at Seoul National University Hospital, Seoul, Korea, Gifu University in Japan, and UCLA Jules Stein Eye Institute, USA. He is currently a Professor of ophthalmology at Seoul National University College of Medicine and a Research Professor at Seoul Artificial Eye Center, Clinical Research Institute, Seoul National University Hospital, Seoul.

Dr. Park is currently member of Association for Research in Vision and Ophthalmology (ARVO), American Academy of Ophthalmology, World Glaucoma Association, Glaucoma Research Society, and Asia Pacific Glaucoma Society.

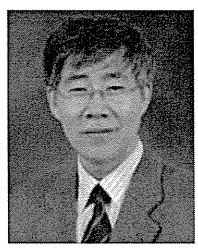

Sun Ha Paek received the Graduate degree from Seoul National University College of Medicine, Seoul, Korea, in 1987, and the Ph.D. degree from the Department of Neurosurgery, Seoul National University College of Medicine, in 1999.

Between 1988 and 1992, he was a Trainee in the Department of Neurosurgery, Seoul National University Hospital, Jongno-gu, Seoul, where he became an Assistant Professor in 1999. He was a Postdoctoral Research Fellow in the Department of Neurology, Cornell University, New York, NY, USA, between 2002 and 2003, and in the Department of Neurosurgery, Medical College of Thomas Jefferson University, Philadelphia, PA, USA, between 2003 and 2004. Since 2005, he has been in charge of Movement Disorder Center, Seoul National University Hospital, where he is currently a Neurosurgeon, and has been a Tenured Professor in the Department of Neurosurgery since 2008. His current research interests include neurooncology and neurodegenerative disease such as Parkinson's disease.

Yasushi Takemura (M'98) received the B.S., M.S., and Ph.D. degrees in electrical and electronic engineering from Tokyo Institute of Technology, Tokyo, Japan, in 1988, 1990, and 1993, respectively.

From 1997 to 1998, he was a Visiting Researcher at Paul Drude Institute for Solid State Electronics, Berlin, Germany. He is currently a Professor in the Division of Electrical and Computer Engineering, Yokohama National University, Yokohama, Japan. He was involved in studying epitaxial thin films of II-VI and III-V compound semiconductors for blue light emitter. His current research interests include magnetic nanostructures, magnetic sensors, and biomedical application of magnetics.

Seongtae Bae (M'99) received the Ph.D. degree in electrical and computer engineering from the University of Minnesota, Minneapolis, USA, in 2003.

He was a Director in the Spintronics and Biomagnetic Sensor Research Division, Waverider, Inc., Minnesota. In 2004, he joined the National University of Singapore (NUS), Singapore, as a Faculty Member. In 2005, he established the Biomagnetics Laboratory (BML), NUS, to support basic applied researches and education in the field of biomagnetics and applied spintronics areas. He is currently involved in the development of biomagnetic sensor for diseases diagnosis, magnetic nanoparticles for biomedical applications, applied spintronics devices, high-density storage and memory devices, and physics of magnetic thin films. His current research interests include magnetic nanoparticles in nanomedicine, nanostructured *in vivo* and implantable magnetic biosensors and systems, magnetically labeled immunoassay biosensors for point-of-care and lab-on-chip disease diagnostics, ultra-low-field detection magnetic sensors for biomagnetism and home security, magnetic thin-film photovoltaic–thermoelectric power generators for a renewable energy system, and nanostructured spintronics for advanced electronics.

Dr. Bae is currently a member of the IEEE Magnetics Society, the IEEE Engineering in Medicine and Biology Society, and the American Physics Society.

J Nanopart Res (2013) 15:1653
DOI 10.1007/s11051-013-1653-y

RESEARCH PAPER

Transfection efficiency influenced by aggregation of DNA/polyethylenimine max/magnetic nanoparticle complexes

Satoshi Ota · Yoshiyuki Takahashi · Asahi Tomitaka · Tsutomu Yamada · Daisuke Kami · Masatoshi Watanabe · Yasushi Takemura

Received: 11 December 2012 / Accepted: 12 April 2013

Abstract Gene delivery using magnetic nanoparticles (MNPs) is known as magnetofection and is an efficient non-viral gene delivery system. γ-Fe_2O_3 nanoparticles (primary diameter = 29 nm) and Fe_3O_4 nanoparticles (primary diameter = 20–30 nm) coated with deacylated linear polyethylenimine (PEI max) were prepared and conjugated with DNA. The dependency of transfection efficiency on the weight of MNPs, viability of HeLa cells, and size of DNA/PEI max/MNP complexes was evaluated. Transfection efficiency initially increased with the weight of the complexes; however, it decreased with further increase in weight. In contrast, cell viability increased with further increase in weight. Cytotoxicity assay showed that the decline in transfection efficiency at higher weights was not attributable to cytotoxicity of DNA/PEI max/MNP complexes. The DNA/PEI max/MNP complexes aggregated because of DNA binding and pH interaction with the medium. Aggregation depending on the weight of MNPs was confirmed. The number of complexes was estimated from the size distribution. In addition, the dependency of the transfection efficiency on aggregation was assessed with respect to cellular endocytic pathways using the complexes. The complexes were internalized through clathrin-dependent endocytosis, which was a size-dependent pathway. This study reveals that decreased transfection efficiency was associated with the extent of aggregation, which was induced by high weight of MNPs.

Keywords Magnetofection · Magnetic nanoparticles · Aggregation · Cytotoxicity · Endocytosis

S. Ota (✉) · Y. Takahashi · T. Yamada · M. Watanabe · Y. Takemura
Faculty of Engineering, Yokohama National University, Yokohama 240-8501, Japan
e-mail: ota-satoshi-gw@ynu.ac.jp

A. Tomitaka
Department of Materials Science and Engineering, University of Washington, Seattle, WA 98195, USA

D. Kami
Department of Cardiac Supports, Kyoto Prefectural University of Medicine, Kyoto 602-8566, Japan

Introduction

Recently, magnetic nanoparticles (MNPs) have attracted considerable attention as transfection vectors. Non-viral transfection vectors such as cationic polymers and cationic liposomes are more biocompatible than viral vectors; however, their transfection efficiency is lower (De Smedt et al. 2000; Guo et al. 2007). MNPs guide DNA into the target tissue and transfect targeted cells rapidly, and the application of magnetic fields leads to the translocation of MNPs inside the cells (Scherer et al. 2002). Coupling non-viral transfection vectors with iron oxide nanoparticles

Published online: 25 April 2013

such as polyethylenimine (PEI) (Scherer et al. 2002), polyamidoamine dendrimer (Pan et al. 2007), and PEI/poly(ethylene glycol)/chitosan copolymer (Kievit et al. 2009)–coated iron oxide nanoparticles facilitate high transfection efficiency and biocompatibility. Furthermore, surface-modified silica (Roy et al. 2005) and gold (Ghosh et al. 2008) nanoparticles have been used instead of iron oxide nanoparticles for gene delivery vectors.

PEI has a cationic charge owing to protonation of the amino nitrogen under physiological conditions (Boussif et al. 1995). PEI conjugates with DNA through electrostatic forces because PEI is cationic and DNA is anionic (Kircheis et al. 2001; Oku et al. 2001). PEI is known as both a coating and a transfection reagent (Boussif et al. 1995; Seino et al. 2009). First, MNPs tend to aggregate because of van der Waals interactions, whereas coating with PEI prevents aggregation via electrostatic repulsion (Seino et al. 2009). Second, DNA/PEI/MNP complexes are guided to cell surfaces by cationic–anionic interactions between PEI and the cell membrane (Payne et al. 2007). Third, the complexes are internalized into the cells by endocytosis promoted by ligand/receptor interactions between PEI and cell surface receptors (Godbey et al. 1999; Scherer et al. 2002). During endocytosis, the complexes are engulfed by cell membrane invaginations and encapsulated into membrane-bound vesicles known as endosomes (Sahay et al. 2010). PEI elicits proton sponge effects characterized by proton accumulation followed by passive chloride influx into endosomes. This influx causes osmotic swelling leading to endosome disruption thereby protecting DNA contained in the complexes from lysosomal degradation (Kichler et al. 2001; Akincl et al. 2005). PEI takes two forms: linear and branched. Linear PEI is less toxic compared with branched PEI (Jeong et al. 2001). In this study, PEI max, which is a deacylated linear PEI, was coated on MNPs. These MNPs were used as transfection vectors. Linear PEI contains residual *N*-acyl groups that hinder gene transfection (Thomas et al. 2005). Deacylation of linear PEI promotes transfection.

With respect to magnetofection, transfection efficiency is determined primarily by magnetic force on the particles, particle configuration in the medium, and endocytic pathway, depending on the size of particles. Magnetic force depends on magnetization, volume, magnetic permeability of MNPs (Pankfurst et al. 2003; Furlani and Xue 2012), and magnetic field gradient (Pankfurst et al. 2003; Akiyama et al. 2010; Furlani and Xue 2012). Configuration of nanoparticles in the medium is influenced by pH, concentration of particles, surface-coating agents, and serum protein (Steitz et al. 2007; Wang et al. 2009; Wigo et al. 2012). The influences of nanoparticle size on endocytosis have been investigated with poly (D, L-lactide-co-glycolide) nanoparticles fractionated to small- (<100 nm) and large-size (>100 nm) nanoparticles (Prabha et al. 2002), gold nanoparticles of size 45, 70, and 110 nm (Wang et al. 2010), and latex fluorescent beads of defined size (50–1000 nm) (Rejman et al. 2004). These studies show that high rate of cellular internalization is achieved with smaller-sized nanoparticles.

The dependency of transfection efficiency on the weight of MNPs was evaluated by determining the cytotoxicity and size of DNA/PEI max/MNPs complexes in HeLa cells. The effect of the size of the complexes on endocytic pathways was also assessed to confirm the influence of size on transfection efficiency. The novelty of this study lies in the confirmation of the MNP weight response of transfection efficiency in terms of cytotoxicity, aggregation of complexes, and endocytic pathway. Moreover, relationships between transfection efficiency and aggregation are confirmed for both γ-Fe_2O_3 and Fe_3O_4 nanoparticles.

Materials and methods

Materials and surface coating

γ-Fe_2O_3 nanoparticles (primary diameter = 29 nm) and Fe_3O_4 nanoparticles (primary diameter = 20–30 nm) were purchased from CIK NanoTek and Nanostructured & Amorphous Materials, Inc. These nanoparticles were coated with PEI max (mw 40,000) purchased from Nacalai Tesque and Polysciences, Inc.

γ-Fe_2O_3 nanoparticles (200 mg) were dispersed in 10 ml solution of 1.0 mg/ml PEI max by supersonification for 10 min. This solution was purified by centrifugation at 743×*g* (*R* = 7.39 cm) for 15 min. The supernatant was centrifuged at 10,000×g (*R* = 8.8 cm) for 30 min. The precipitate was collected as PEI max-coated γ-Fe_2O_3 nanoparticles (Kami et al. 2011a). For Fe_3O_4 nanoparticles,

200 mg of nanoparticles were dispersed in 40 ml solution of 1.0 mg/ml PEI max. The rest of the process was the same as for γ-Fe_2O_3 nanoparticles.

Transfection and preparation of MNP of different densities

HeLa cells from a human cervical carcinoma line were cultured in Dulbecco's modified Eagle medium (DMEM) supplemented with 10 % fetal bovine serum (FBS) and 1 % penicillin–streptomycin (PS). The cells were seeded in 35 mm dishes at a density of 200,000 cells/well on the day prior to transfection. The cells were incubated at 37 °C in a humidified atmosphere containing 5 % CO_2.

To evaluate the dependency of transfection efficiency on the weight of MNPs, solutions of 1 mg/ml PEI max and various densities of PEI max-coated MNPs were prepared. PEI max and PEI max-coated MNPs solutions (7.5 μl) were mixed with 2.5 μg of plasmid DNA expressing enhanced green fluorescent protein (EGFP) in sterile water for 15 min. DNA/PEI max complexes and DNA/PEI max/MNP complexes were added to 1 ml medium. Each medium containing DNA/PEI max complexes or DNA/PEI max/MNP complexes was added to the cells in each sample dish after removing the medium and washing the cells with phosphate-buffered saline (PBS). The weights of PEI max-coated MNPs in each 7.5 μl sample of 1 mg/ml PEI max solution were 0.75, 1.5, 2.25, 3.0, 4.5, and 7.5 μg for both γ-Fe_2O_3 and Fe_3O_4. The amount of plasmid DNA was 2.5 μg for all the samples.

Each dish containing DNA/PEI max/MNP complexes was placed on a neodymium (NdFeB) permanent magnet (diameter = 40 mm, height = 20 mm) purchased from Sangyo Supply Co. for 1 h. Each dish containing DNA/PEI max/MNP complexes was excited using a magnetic field gradient perpendicular to the dish at 26.5–33.0 T/m in the area of the dish near the cell surface. Two days after transfection, its efficiency was evaluated by fluorescence microscopy. The areas of fluorescent cells in fluorescence micrographs were compared with those of all cells observed in phase-contrast micrographs. The ratio of area of the fluorescent cells was calculated. Nine datasets were prepared for each condition of the fluorescence micrographs (three dishes prepared for each condition and three sites observed in each dish).

Cytotoxicity assay

HeLa cells were seeded in 35 mm dishes at a density of 200,000 cells/well. One day after the incubation, PEI max, PEI max-coated MNPs, DNA, DNA/PEI max complexes, and DNA/PEI max/MNP complexes were added to each dish. The method of transfection and preparation of each MNP density was the same as that for the transfection experiment. Two days after incubation, cell viability was evaluated by trypan blue dye exclusion test.

Size measurement

The hydrodynamic sizes of the PEI max-coated γ-Fe_2O_3 and Fe_3O_4 nanoparticles were measured by dynamic light scattering (DLS) method using a fiber-optical particle analyzer (FPAR-1000, Otsuka Electronics). The morphologies of the PEI max-coated γ-Fe_2O_3 nanoparticles and DNA/PEI max/γ-Fe_2O_3 nanoparticle complexes were characterized by transmission electron microscopy (TEM).

Endocytic inhibitors

Chlorpromazine and genistein were used as endocytic inhibitors. Chlorpromazine (Nacalai Tesque) inhibits clathrin-dependent endocytosis (CDE), and genistein (Nacalai Tesque and Fujicco Co.) inhibits clathrin-independent endocytosis (CIE).

In the transfection experiment, HeLa cells (200,000 cells/well) were seeded in 35 mm dishes on the day prior to the initiation of the inhibition study. The cells were preincubated with endocytic inhibitors (10 μg/ml chlorpromazine or 200 μM genistein) in 1 ml/well of medium for 30 min. Endocytic inhibitors were also added during magnetofection and incubated for 1 h after magnetofection. Chlorpromazine was diluted in sterile water, and genistein was diluted in dimethyl sulfoxide (DMSO) so that the final concentration of DMSO in the medium was <0.1 % (Gruenstein et al. 1975; Rejman et al. 2005; Vercauteren et al. 2011).

Results and discussion

Dependency of transfection efficiency on weight of MNPs and cytotoxicity assay

Figure 1 illustrates the dependency of transfection efficiency on the weight of γ-Fe_2O_3 and Fe_3O_4 nanoparticles. Transfection efficiency increased with weight, but decreased with further increases in γ-Fe_2O_3 and Fe_3O_4 (>1.5 μg). This dependency has been reported elsewhere (Plank et al. 2003; Kami et al. 2011a). For the weight of 1.5 and 2.25 μg (γ-Fe_2O_3) and 1.5, 2.25, and 3.0 μg (Fe_3O_4), differences in transfection efficiency were not significant ($p \geq 0.05$). The transfection efficiency of γ-Fe_2O_3 nanoparticles was higher compared with that of Fe_3O_4 nanoparticles at 0.75, 1.5, and 2.25 μg ($p < 0.05$). Figure 2 is fluorescent micrographic images of γ-Fe_2O_3. These images also indicated the trend of transfection efficiency shown in Figs. 1 (2).

Figure 3 illustrates the viability of HeLa cells exposed to PEI max, PEI max-coated γ-Fe_2O_3 nanoparticles, DNA, DNA/PEI max complexes, and DNA/PEI max/γ-Fe_2O_3 nanoparticle complexes. The weight of MNPs was 2.25 μg (Fig. 3). The reduction in cell viability in cells exposed to PEI max and DNA compared with the control sample without PEI max, MNPs, or DNA was negligible ($p \geq 0.05$). The cell viability of the sample with PEI max-coated MNPs, DNA/PEI max complexes, and DNA/PEI max/MNP complexes decreased in contrast to the sample with only PEI max ($p < 0.05$). In addition, viability decreased significantly in the sample with DNA/PEI/max MNP complexes in comparison with the sample containing only DNA ($p < 0.05$). Figure 4 illustrates the dependency of cell viability on the weight of MNPs. Cell viability initially decreased with weight of MNPs; however, it increased with further increase in MNP weight (above 2.25 μg; $p < 0.05$).

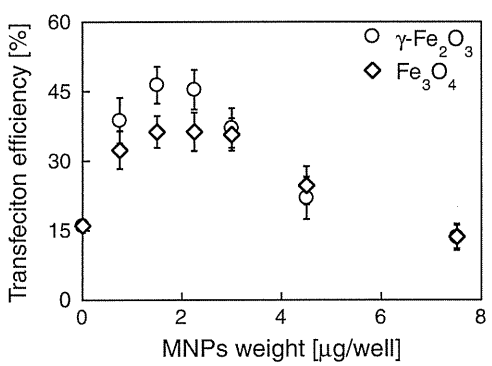

Fig. 1 Transfection efficiency as a function of magnetic nanoparticles (MNP) weight. Transfection efficiency was evaluated by fluorescent microscopy. MNP weight of 0 μg/well indicates the sample containing DNA/polyethylenimine (PEI) max complexes

Decline in transfection efficiency has been attributed to cytotoxicity of DNA/MNPs (Plank et al. 2003). However, Figs. 1 and 4 show that cell viability in contrast to the decline in transfection efficiency, increased at higher MNP weights. In addition, the γ-Fe_2O_3 nanoparticle without coating has been reported to be of low cytotoxicity (Lee et al. 2011). It has been also reported that linear PEI has low cytotoxicity at lower concentrations, but is cytotoxic at higher concentrations (Banerjee et al. 2006; Jeong et al. 2001). In this study, the cytotoxicity of HeLa cells that were exposed to PEI max was significantly low because PEI max was used in low concentrations. Decline in cell viability in PEI max-coated γ-Fe_2O_3 nanoparticles is induced by reactive oxygen species due to the formation of free hydroxyl radical species, reacting with a range of intracellular constituents, due to high internalization of γ-Fe_2O_3 nanoparticles (McCord 1998; van der Bos et al. 2003; Arsianti et al. 2010b). However, this decline was minor because of the low doses of MNP incorporated into cells. Figures 3 and 4 suggest that the cytotoxicity may be attributed to high internalization of DNA/PEI max/MNP complexes into cells. The toxicity of DNA per se was negligible (Fig. 3). Internalization of DNA/PEI max/MNP complexes decreases cell viability, probably because of the disruption of cell membrane integrity after internalization (Prijic et al. 2012). The viability of HeLa cells exposed to complexes that contained γ-Fe_2O_3 nanoparticles of 2.25 μg was reduced despite the low cytotoxicity of PEI max-coated γ-Fe_2O_3 nanoparticles. The sample with MNPs of 2.25 μg induced higher transfection efficiency. This result suggests that cytotoxicity was because of higher internalization of DNA/PEI max/MNP complexes, and the trade-off between transfection efficiency and cytotoxicity is indicated (Arsianti et al. 2010b). The dependency of transfection efficiency and cell viability on the weight of MNPs indicates that transfection efficiency was not reduced because of cytotoxicity.

Aggregation of PEI max-coated MNPs

Figure 5 illustrates the size distribution of PEI max-coated γ-Fe_2O_3 and Fe_3O_4 nanoparticles in sterile